Peer reviewed version

Link to published version (if available):
10.1038/s41565-018-0085-3

Link to publication record in Explore Bristol Research
PDF-document

University of Bristol - Explore Bristol Research
General rights

Nanoparticle induced neuronal toxicity across placental barriers is mediated by autophagy and dependent on astrocytes

Simon J Hawkins [1, 2], Lucy A Crompton [1, 3,] Aman Sood [2] Margaret Saunders [4], Noreen Boyle [5], Amy Buckley [5], Aedin M Minogue [5], Sarah F. McComish [5] Natalia Jimenez Moreno [3], Oscar Cordero-Llana [1], Petros Stathakos [1], Stephen Kelly [6], Jon D Lane [3], C. Patrick Case [2], and Maeve A Caldwell [5*]

1. Regenerative Medicine Laboratory, School of Clinical Sciences, University of Bristol, University Walk, Bristol, BS8 1TD, UK

2. Musculoskeletal Research Unit, School of Clinical Sciences, University of Bristol, Southmead Hospital, Bristol, BS10 5NB, UK

3. Cell Biology Laboratories, School of Biochemistry, University of Bristol, University Walk, Bristol, BS8 1TD, UK

4. Department of Medical Physics & Bioengineering, St Michael's Hospital, University Hospitals Bristol NHS Foundation Trust, Bristol, BS2 8EG, UK

5. Trinity College Institute of Neuroscience, Department of Physiology, Trinity College Dublin, Dublin 2, Ireland

6. New Jersey Neuroscience Institute, JFK Medical Centre, NJ 08818, USA

* email: maeve.caldwell@tcd.ie

Abstract

The potential for maternal nanoparticle exposures to cause developmental toxicity in the fetus without the passage of nanoparticles has previously been shown. We now demonstrate that exposure of CoCr nanoparticles to BeWo cell barriers, a human in vitro model of the human placenta, triggers an impairment of autophagic flux and the release of the proinflammatory factor IL-6. This contributes to an altered differentiation of human neuroprogenitor cells plus DNA damage in the derived neurons and astrocytes that is mediated by the astrocytes. Inhibiting autophagic degradation in the BeWo barrier by overexpression of a dominant-negative human ATG4B[C74A] significantly reduces the levels of DNA damage in astrocytes. In vivo, indirect nanoparticle toxicity in mice also results in neurodevelopmental abnormalities with reactive astrogliosis and increased DNA damage in the fetal hippocampus. This demonstrates the potential importance of autophagy in eliciting nanoparticle toxicity and the risk of indirect developmental neurotoxicity following maternal nanoparticle exposure.

Article

Nanoparticles (NPs) are being increasingly used in drug delivery, chemotherapy, imaging and diagnostics due to their ability to travel within organisms by utilising cellular pathways (Anselmo and Mitragotri, 2016). During their interactions with cell membranes, and internalisation into cells, key signalling pathways and processes are altered (Saei et al., 2017). In addition to affecting the health of directly exposed cells, the internalization of NPs can also detrimentally affect neighbouring cells in a manner similar to the radiation induced bystander effect (Thubagere and Reinhard, 2010).

In bilayered BeWo in vitro models of the placental barrier it has been shown that biopersistent NPs are internalised into the upper trophoblast cell layer triggering intercellular signalling (Bhabra et al., 2009; Sood et al., 2011). The exposed barriers undergo increased Connexin-43 (CX43) dependent signalling that leads to the secretion of factors such as ATP. These factors can then detrimentally

2

affect fibroblasts and differentiating human Embryonic Stem (hES) cells remote from this barrier. This "indirect" toxicity does not occur when single layered barriers are exposed to NPs and is not due to the passage of the degradation products of NPs. In pregnant mice exposure to CoCr NPs at E12.5 also causes increased levels of DNA damage in the blood and livers of their progeny without NPs crossing the placenta (Sood et al., 2011).

The most common developmental abnormalities in humans due to the maternal exposure to toxins, relate to neurodevelopment (Grandjean and Landrigan, 2014). Studies have shown this is also likely the situation for biopersistent NP exposures during pregnancy (Shimizu et al., 2009; Hougaard et al., 2010; Mohammadipour et al., 2014). It has been found that NPs can cause reduced cell proliferation in the fetal hippocampus, impaired learning and memory (Mohammadipour et al., 2014), altered expression of genes related to brain development (Shimizu et al., 2009), and neurobehavioural abnormalities (Hougaard et al., 2010). These changes have been considered to occur due to the transfer of NPs or their degradation products across the placenta to the fetus (Mohammadipour et al., 2014). It has, however, been shown that NPs can cause intrauterine growth restriction (Yamashita et al., 2011) and developmental abnormalities without crossing the placenta (Sood et al., 2011). The importance of the placenta for fetal brain development has also been shown (Goeden et al., 2016).

Here we show that the signalling cascade, triggered by biopersistent NPs in the BeWo model of the placenta and involving the cytokine IL-6, causes DNA damage in differentiating neural progenitor cells. The initiation of this signal is mediated by autophagy while the resulting DNA damage in neurons is dependent on the presence of astrocytes. Inhibiting the autophagy response to the application of NPs in the BeWo barrier, by lentiviral transduction with dominant-negative human ATG4B^{C74A}, significantly reduces the levels of DNA damage in astrocytes. Finally in vivo, we demonstrate that maternal NP exposure at E12.5 results in reactive astrogliosis and increased DNA damage in the neonatal hippocampus.

Results

CoCr NPs alter autophagic flux in BeWo models of the placenta.

BeWo cells, a human trophoblast choriocarcinoma derived cell line, were grown on transwell inserts for 7 days so as to form confluent bilayered cell barriers (Figure 1a) (Bhabra et al., 2009). BeWo cell barriers are widely used as in vitro models of the placental barrier to study placental endocrine function and transplacental transport of substances such as drugs, amino acids, immunoglobulins, fatty acids, transferrin and viruses (Li et al., 2013; Bode et al., 2006). These cells were exposed to NPs of cobalt and chromium (CoCr) surgical alloy, as humans are exposed internally to CoCr nanoparticles by wear mechanisms associated with metal-on-metal (CoCr) orthopaedic joint replacement (Polyzois et al., 2012). CoCr NPs are known to have genotoxic and cytotoxic effects in human tissue culture if they are added directly to cells in culture (Papageorgiou et al., 2007). However, when BeWo barriers are exposed to a low concentration of CoCr NPs (0.04 mg/ml) the barriers remain intact, shown by unaltered trans epithelial electric resistance (TEER) measurements (Figure 1b), and NPs fail to traverse to the basolateral milieu (Bhabra et al., 2009; Sood et al., 2011). Instead, the NPs are internalised into the upper layer of the barriers, triggering an increased barrier stress response characterised by the impairment of mitochondrial activity (See Fig S1). A DNA damaging signal is transmitted from the barrier that results in greater levels of DNA damage in exposed cells than if the same amount of NPs were exposed to the cells directly (Bhabra et al., 2009; Sood et al., 2011).

We now show that P53 expression levels are elevated in NP-treated barriers, whereas HSP70 expression remains unaffected (Figure 1c & d). As mitochondrial inhibition due to oxidative stress has been shown to induce autophagy via p53 (Crighton et al., 2006), the levels of autophagic activity were also determined. Western blot analysis revealed increased protein expression for LC3-II and P62 indicating a build up of autophagosomes associated with a blockade of

autophagosome clearance (Figure 1c, e & f) (Klionsky et al., 2016). This was found to occur predominantly in the upper layer of the barrier where NPs accumulate following internalisation (Figure 1j & k) (Sood et al., 2011. When the lysosomal blocker bafilomycin A1 (Klionsky et al., 2016) was added (Figure 1i & l), an increase in LC3 positive puncta and P62 staining intensity was recorded upon barrier immunostaining (Fig 1g - l). NP exposure therefore results in altered autophagic flux, with a partial blockade of autophagosomal clearance likely due to impaired lysosomal function, in a similar fashion to the effects of gold and polystyrene NPs (Ma et al., 2011).

Indirect NP exposure causes DNA damage in human astrocytes and neurons.

To investigate the effect of the DNA damaging signalling on neural cell lineage differentiation, media was conditioned under the BeWo barrier during NP exposure then transferred onto differentiating NPCs (See Figure S2). These were derived from the human fetal cortex and differentiated in culture to form neurons and astrocytes (See Figure S3a) (Svendsen et al., 1998). Results showed that exposure to conditioned media had no effect on cell survival (See Figure S4); however, immunostaining revealed a phenotypic shift towards glial cell differentiation (See Figure S3b). These glial cells were immunostained with GFAP and their astrocyte identity was confirmed by co-staining with EAAT1 (See Figure S5). A marked change in the morphology of the astrocytes was also seen, evidenced by increased nuclear and cytoplasmic areas (Figure 2a-f). The neurons in culture with the astrocytes did not show obvious morphological changes (data not shown). The phenotypic changes found in the astrocytes suggest that they may have become reactive; although qPCR analysis revealed similar expression levels of *GFAP* compared to the barrier control (See Figure S6 (Sofroniew, 2014).

The changes found in astrocytes were not due to oxidative stress (See Figure S4b); therefore we looked for evidence of astrocytic DNA damage responses. γ-H2AX immunostaining was performed to identify double stranded DNA breaks in neuronal/astrocytic cultures co-stained for either TUJ1

or GFAP (Dickey et al., 2009). When a double stranded DNA break occurs, H2A histone family member X (H2AX), becomes extensively phosphorylated at serine -129, and forms foci at break sites referred to as γ-H2AX foci (Paull et al., 2000). Immunostaining for γ-H2AX revealed an increase in the numbers of γ-H2AX foci in our exposure group in both astrocytes and neurons, but with a more pronounced affect in astrocytes (Figure 3a, c) than in neurons (Figure 3b, d and e). Increased γ-H2AX foci formation in astrocytes also occurred following barrier exposure to 0.04mg/ml TiO2 NPs (See Figure S7). However exposure to 5% [w/v] F127 NPs, which are under investigation for drug delivery to the brain, did not induce the same increase in astrocyte γ-H2AX foci (See Figure S8) (Yamashita et al., 2011; Sood et al., 2011; Basak and Bandyopadhyay, 2013).

The formation of γ-H2AX foci in neurons dependson astrocytes.

Investigations were next performed to determine whether the astrocytes might be influencing any toxic effect on the neurons in culture. An established mechanism by which astrocytes mediate neuroprotection is by the production of glutathione (GSH) (Chen et al., 2001). GSH-glo assay assessment demonstrated a large increase in GSH in the culture medium (See Figure S9); however, when primary cultures that were characterised as >99% neuronal (see Figure 4a) were exposed, only low background levels of γ-H2AX foci were detected in neurons, with no difference in comparison to controls (Figure 4b). Also, when an additional stage of media conditioning was introduced – in which the media was first placed onto cultures of astrocytes derived from human neural progenitors – increased levels of DNA damage were once again observed in primary neurons (Figure 4c). We therefore concluded that the formation of γ-H2AX foci in the primary neurons was dependent on the presence of astrocytes in culture.

As astrocytes appear later in embryonic development than neurons, we next investigated whether the indirect toxicity we observed was a stage specific effect only occurring once astrocytes have differentiated (Barnabe-Heider et al., 2005). To test this we utilised a hES cell line to generate the primitive germ layers, including the neuroectoderm as occurs in the very early embryo (Pal et al.,

2011). An embryoid body (EB) model was used to induce germ layer differentiation and we examined expression of *P53* by qPCR (Pal et al., 2011). No increase in the expression of *P53* was observed which suggests that at this early stage of differentiation there is no activation of DNA damage pathways (Figure 4d). Furthermore no difference was found in the expression of the neuroectoderm markers *NESTIN* or *SOX1* during gene expression profiling (Figure 4d), or flow cytometry assessment (See Figure S10), indicating that exposure to BeWo conditioned media in the presence of NPs does not affect early neural differentiation (Pevny et al., 1998).

DNA damaging signalling and initialisation in the BeWo barrier

Further experiments were performed to try to further establish the mechanism by which the DNA damaging signalling is communicated to astrocytes. In Sood et al., it was believed that the signalling was transmitted via a burst of ATP from the barrier plus an additional vesicular release of protein (Sood et al., 2011). As ATP was unlikely to have an ongoing effect past the initial application of conditioned media to NPCs, we examined the release of a number of chemokines/cytokines, namely, RANTES, GM-CSF, TNFα and IL-6, using enzyme-linked immunosorbent assays. ELISAs were performed on media conditioned by the BeWo barrier and also from astrocytes that had been exposed to media from the BeWo barrier. TNFα and IL-6 were found to be secreted by the BeWo barrier; however, RANTES and GM-CSF were below the limit of detection. TNFα secretion did not increase following exposure of the BeWo barrier to NPs, or following culture of NPC derived astrocytes (See Figure S11). IL-6 secretion from the BeWo barrier following NP exposure did however significantly increase (See Figure S12), and remained significantly elevated following culture of NPC derived astrocytes (Figure 4e). The role of IL-6 in the initiation of DNA damage was further investigated by transducing the BeWo barrier with two different lentiviral vectors expressing an IL-6 Sh-RNA. TEER measurements confirmed barrier integrity post lentivirus and CoCr NP exposure (See Figure S13). IL-6 reduction was confirmed by ELISA (See Figure S14), media was transferred onto differentiating NPC's and γ-H2AX

immunostaining was performed. Significantly reduced levels of γ-H2AX were recorded in GFAP positive astrocytes (Figure 4f). exposed to media from barriers treated with Sh-IL-6 and GFAP negative cells (See Figure S15). In order to obtain further confirmation of the role of IL-6 we utilised an IL-6 blocking antibody with relevant isotype (IgG) control and obtained similar results (Figure 4g); blockade of IL-6 was confirmed by ELISA (See Figure S16). Interestingly a medium mediated DNA damage repair response, following ionizing radiation, has been correlated with the release of cytokines such as IL-6 in human fibroblasts (Dieriks et al., 2010).

The role of autophagy in the initiation of the DNA damage was then further investigated by transducing the BeWo barrier with a lentiviral vector expressing dominant-negative human GFP-ATG4B[C74A] (Fujita et al., 2008; Betin et al., 2013). ATG4B is the major ATG4 family protease required for priming and subsequent delipidation of ATG8 paralogues, including LC3. ATG4B[C74A] overexpression hampers LC3 lipidation and inhibits autophagic degradation due to defective autophagosome closure (Fujita et al., 2008). Lentiviral uptake was confirmed using confocal microscopy for GFP in the BeWo barriers and TEER measurements confirmed barrier integrity post CoCr NP exposure (See Figure S17). Media was then transferred onto differentiating NPCs and γ-H2AX immunostaining was performed on the astrocytes in culture. Significantly reduced levels of γ-H2AX foci were recorded in astrocytes exposed to media from autophagy-impaired barriers, indicating that autophagy has a key role in the initialisation of the DNA damaging signalling (Figure 4h).

To begin to understand the possible links between autophagy and DNA damage signalling in our barrier model, we measured IL-6 levels in media derived from autophagy-impaired barriers treated with NPs (See Figure S18 & S19). Autophagic activity has previously been linked to the IL-6 biosynthetic pathway (Maycotte et al., 2015) where a novel mTOR-enriched autolysosomal compartment has been implicated in the control of IL-6 secretion in diverse cellular systems (Narita et al., 2011). Our ELISA data revealed that barriers exposed to NPs in the presence of ATG4B[C74A] released less IL-6 than control GFP-expressing barriers (See Figure S18); a finding consistent with

the requirement for autophagy during IL-6 release in an airway epithelial model of ultrafine particle-induced inflammation (Chen et al., 2016). Barriers treated with BafA1 also secreted significantly less IL-6 than control treated barriers in the absence and presence of NPs (See Figure S19). These data support a model in which the impaired, but not wholly inhibited autophagic flux activity seen in barriers treated with NPs, promotes the robust IL-6 release that we have recorded.

IL-6 is a keystone cytokine in health and disease (Hunter and Jones, 2015). Anti-IL6 therapies are used to treat inflammatory conditions such as rheumatoid arthritis and have been investigated to treat various cancers (Mauer et al., 2015). In the nervous system IL-6 has been shown to be a broad mediator of neuroinflammation and is thought to have a role in the generation of reactive astrocytes (Campbell et al., 1993) However, it also has important roles in maintaining neural health including being a required signalling component of astrocyte neuroprotective effects in various CNS insults (Shinozaki et al., 2017; Haroon et al., 2011; Drogemuller et al., 2008). In our experimental conditions, IL-6 contributes to a neurotoxic effect rather than a neuroprotective effect, emphasising how the versatile role of IL-6 in neural health and disease requires further investigation (Rothaug et al., 2016).

Nanoparticle exposure results in fetal neurodevelopmental abnormalities.

In vivo exposures to NPs were then performed in pregnant mice to assess the potential for NPs to indirectly cause developmental neurotoxicity as previously described (Sood et al., 2011). Mice were intravenously injected with CoCr nanoparticles at two stages of pregnancy: 9.5 days, when the exchange of nutrients is performed by the uterus and yolk sac; and 12.5 days, when the placenta is fully established with three layers (Simmons et al., 2008). In our original experiments significant levels of Co and Cr did not increase in the neonates, nor were any pathological changes noted in the placenta or in the neonates visceral organs; however, increased DNA damage was found in neonatal blood and liver (Sood et al., 2011). Here, we analysed a number of astrocytic genes in whole brain samples that have previously been shown to be upregulated in astrocytes in

response to stress/injury (Hennessy et al., 2015; Liddelow et al., 2017; Zamanian et al., 2012). *GFAP* expression, which is increased by astrocytes in response to neurological insults (Sofroniew, 2014), was significantly increased in the E12.5 NPs-injected group when compared to all other groups (CoCr effect: F = 6.120; P=0.030.01 and embryonic age effect: F = 5.409; P = 0.048) (Figure 5a). In contrast, no differences in *GFAP* expression were recorded in the E9.5 NPs-injected group, highlighting the stage-specific affects of NP exposure during pregnancy. Expression of the astrocytic activation markers *STEAP4* and *PTX3* (Hennessy et al., 2015) however did not alter significantly at either time-point of NP exposure in whole brain when compared to relevant control groups (See Figure S20).

Given that *GFAP* mRNA levels were increased, we next carried out immunohistochemical staining for this marker. Results showed that there was a significant increase in GFAP immunostaining in the hippocampus when NPs were injected at E12.5 (Figure 5b-d), as well as elevated *STEAP4* mRNA levels (Figure 5e) though not *PTX3* (See Figure 21). Immunohistological staining of the hippocampus in the E12.5 treated animals also identified significantly increased γ-H2AX foci (CoCr effect: F = 14.13; P=0.0032 and embryonic age effect: F = 5.878; P=0.0337; (Figure 5f & See Figure S22).

In summary we have shown the importance of autophagy in nanoparticle pathogenesis and that biopersistent NPs can cause developmental neurotoxicity across placental barriers. We have shown that astrocytes are key mediators of this neurotoxicity and that the fetal hippocampus is particularly affected in mice in vivo.

Discussion

The placenta is the vital support unit for the fetus and has an essential role in modulating fetal brain development (Muller et al., 2017; Goeden et al., 2016).

During periods of stress due to food deprivation, autophagy may be upregulated in the placenta to protect the fetal brain (Broad and Keverne, 2011). However, dysfunction of autophagy within the placenta is also linked to conditions such as intra-uterine growth restriction and neonatal encephalopathy (Avagliano et al., 2013). The autophagic and endo-lysosomal pathways are frequently altered by NP exposure to cells (Stern et al., 2012), exposure of CoCr NP to the BeWo trophoblast barriers caused autophagy dysfunction and triggered the release of IL-6. Inhibiting autophagic degradation in the BeWo barrier, by performing a transduction of a lentiviral vector containing human ATG4B^{C74A}, significantly reduced levels of DNA damage in astrocytes. These results suggest that dysfunctions of autophagic pathways may be important for the initiation of NP induced DNA damaging signalling in BeWo trophoblast barriers.

We also show that the astrocytes in exposed cultures did not provide neuroprotection to neurons and were instead neurotoxic. Furthermore, in vivo maternal NP exposure resulted in reactive astrogliosis and increased DNA damage in the neonatal hippocampus. The role of astrocytes in disease is increasingly becoming evident, they modify neuronal activity as part of the tripartite synapse, but can also cause neurotoxicity and may be involved in neurodegenerative conditions and epilepsy (Sofroniew, 2014). During development astrocytes and neurons have specific neuroglial signalling that is important for the promotion of synaptogenesis and neuronal network remodelling (Sun et al., 2013). We postulate that exposure of the human placenta to biopersistent NPs could initiate a signalling cascade, that perturbs the important relationship between astrocytes and neurons during neurodevelopment. We therefore argue that maternal NP exposure during pregnancy should if possible be avoided, even if the NPs themselves are not thought to cross the placenta to the fetus.

Materials and methods

Barrier model setup

BeWo cells were grown on transwell inserts for 7 days to form confluent bilayered layers of the cells (Figure 1a). BeWo b30 cells were obtained from Dr Margaret Saunders (University Hospitals Bristol NHS Foundation Trust, Bristol, UK) with permission from Dr Alan Schwartz (Washington University St. Louis, MO). This cell line was authenticated by the European Cell and Culture Collection and were tested every two months for mycoplasma contamination. Cells were cultured in Dulbecco's Modified Eagle's Nutrient Mixture (DMEM) F-12 Ham with phenol red and supplemented with 1% L-Glutamine-Penicillin-Streptomycin, 1% amphotericin B solution and 10% Fetal Bovine Serum (Sigma-Aldrich) in a humidified incubator at $37^{\circ}C$ in 5% CO_2. They were seeded at 10^5 cells/cm^2 on polyester 0.4µm pore membranes on a Transwell® insert (Appleton Woods, Birmingham, UK) and grown for 7 days during which they had regular media changes (Bode et al., 2006). After 7 days they form a confluent barrier of 2-3 cells in thickness at which point the CoCr NPs are applied in serum free media above the barrier for 24 hours. During this the NPs are internalised into the upper layer of the BeWo barrier (Bhabra et al., 2009). Tissue culture media is conditioned below the barrier in the basal chamber during this period and is subsequently used in media transfer experiments (Suppl Fig 2). Serum is omitted from the NP media due to the potential for it to transfer to the basal chamber (Bhabra et al., 2009), as it is known to drive neural progenitor cell differentiation to a glial lineage (Ostenfeld and Svendsen, 2003). The integrity of the barrier before and after application of NPs was confirmed using Trans-Endothelial Electrical Resistance (TEER) measurements using an EVOM volt-ohmmeter with a 12mm Endohm unit.

Lentiviral inhibition of autophagy

Lentiviral vectors containing human ATG4B[C74A] with an N-terminal GFP tag or GFP alone were produced in pxlg3-gfp (a modified pSEW sin vector kindly provided by Dr G. Cory, University of Exeter) (Fujita et al., 2008; Betin et al., 2013). Lentiviruses were generated by co-transfection with the envelope plasmid pMD.G and the packaging plasmid pCMVR8.91 in HEK 293T cells (Danson et al., 2007).

Preparation of nanoparticles

The 80 ± 14.6 nm CoCr NPs were produced by a thermal plasma method (Suppl methods and Suppl Table 1). Prior to use they were sonicated using a Sonics VibraCELL VC130PB sonicator after which they were applied to the upper chamber of the barrier model at a concentration of 0.04mg/ml. This exposure level has previously been found not to cause transition of CoCr NPs across the BeWo barrier (Bhabra et al., 2009; Sood et al., 2011).

Human neural progenitor cell culture

Human fetal cortical neural progenitor cells (NPCs) were derived from 8-12 week human fetuses following elective termination of pregnancy under ultrasound guidance in accordance with the Polkinghorne and Department of Health guidelines, with full ethical committee approval and under the Cardiff University Human Tissue Act 2004 research licence. NPCs cells were cultured in poly-HEMA coated tissue culture flasks in a non-adherent fashion as neurospheres and passaged, by chopping using a McIlwain tissue chopper set to an interval of 200µm every 10 days as we have previously described (Svendsen et al., 1998). They were cultured in media composed of DMEM and F 12 glutamax (7:3 ratio) with 0.7% glutamax, 1% penicillin-streptomycin, 2% B27 (sigma) and 1:1000 FGF2, 1:1000 EGF and 1:1000 Heparin (Peprotech). To study the effects on NPC differentiation from the conditioned media neurospheres were dissociated using accutase (Sigma) then placed in media without mitogens. 10^5 cells were then seeded onto 13mm PDL/laminin coated glass coverslips and allowed to adhere for 24 hours after which their media was replaced with NPC differentiation media conditioned in the BeWo barrier model then cultured until day 7 of differentiation.

hES cell culture and formation of embryoid bodies

Shef 3 hES cells were obtained under licence from the UK stem cell bank and cultured on mitotically inactivated Mouse Embryonic Fibroblasts. Cells were maintained in Knock Out-DMEM, 20% Knock-out Serum Replacer (KSR), 1% NEAA, 2 mM Glutamax, 0.1 mM ß-Mercaptoethanol, and 1% penicillin and streptomycin (Life Technologies) supplemented with 10 ng/ml FGF2 (Peprotech). The cells were passaged manually. EBs were formed by detaching 25

undifferentiated colonies from 8 hES cells plates by applying 1mg/ml Collagenase IV (Life Technologies) for 30 minutes at 37°C. Once detached the colonies were washed in DPBS then chopped into 200µm uniform pieces using McIlwain tissue chopper (Mickle Engineering, Gomshall, U.K.). They were then placed in Poly-HEMA coated flasks (Sigma) to prevent cell attachment and re-suspended in media without FGF2. These hES cell colony pieces were allowed to differentiate in non-adherent culture for 4 days until they had developed into spheres known as EBs. At this stage the EBs were removed from their media and placed in EB media that had been conditioned beneath the BeWo barrier. The EBs were removed from this media on day 7 then total RNA was extracted.

In vivo experiments.

The Seton Hall University Institutional Animal Care and Use Committee approved animal experiments. Adult mice (C57Bl/6; 8 weeks old) were maintained in 12h light/dark cycles with free access to food and water. Female mice were mated with male mice overnight and pregnant females were designated embryonic day 0.5 (E0.5) by the presence of a vaginal plug the next morning. Pregnant females were randomly selected and CoCr NPs were injected intravenously into their jugular vein at either E9.5 or E12.5 in 100µl of sterile saline at a dose of 0.12mg per mouse. Controls mice were injected with sterile saline only on either E9.5 or E12.5. Newborn pups (postnatal day zero, P0) were anesthetized with isoforane in a small chamber, transferred to a sterile petri dish and placed on a frozen ice-pack. The heart was rapidly exposed and pups transcardially perfused with 2ml of DepC treated phosphate buffered saline (PBS). Half of the pups then had their brains removed and immediately immersed in RNA later, the other half were transcardially perfused with 5 ml of paraformaldehyde (4%, made with DepC treated PBS). The brains of PFA perfused pups were also removed and placed in PFA for 24 hours then stored in PBS until used. Brains were cryoprotected by immersing in 30% sucrose then sectioned at 20µm and stored at -80°C until further analysis; a minimum of 3-4 brains were sectioned per treatment group.

γ-H2AX immunostaining assessment of DNA breaks

Immunostaining for γ-H2AX foci was used to identify double stranded DNA breaks in NPC cells (Paull et al., 2000; Dickey et al., 2009). This was detected by immunocytochemistry labelling using rabbit anti phosphorylated H2A.X (Ser139) (Cell Signalling Technology, ♯9718) 1:500 primary antibody. 100 cells were imaged per biological replicate using an Olympus BX-41 microscope with ISIS capturing and analysing system (Metasystems). Greater than 4 foci were taken as a measure of significant DNA damage in keeping with accepted protocols (Sood et al., 2011; Bhabra et al., 2009).

Statistical analysis

Statistical analysis was performed using one-way followed by Newman Keuls post hoc test or a two-way ANOVA with Bonferroni post hoc test for multiple comparisons or unpaired T tests (two tailed) with Graphpad prism statistical software.

Please see supplementary section for further methods.

Data availability: The data that support the findings of this study are available form the corresponding author upon reasonable request.

References

Anselmo, A. C. & Mitragotri, S. 2016. Nanoparticles in the clinic. *Bioengineering & Translational Medicine,* 1(1)**,** pp 10-29.

Avagliano, L., Danti, L., Doi, P., Felis, S., Guala, M., Locatelli, A., . . . Bulfamante, G. P. 2013. Autophagy in placentas from acidotic newborns: an immunohistochemical study of LC3 expression. *Placenta,* 34(11)**,** pp 1091-4.

Barnabe-Heider, F., Wasylnka, J. A., Fernandes, K. J., Porsche, C., Sendtner, M., Kaplan, D. R. & Miller, F. D. 2005. Evidence that embryonic neurons regulate the onset of cortical gliogenesis via cardiotrophin-1. *Neuron,* 48(2)**,** pp 253-65.

Basak, R. & Bandyopadhyay, R. 2013. Encapsulation of hydrophobic drugs in Pluronic F127 micelles: effects of drug hydrophobicity, solution temperature, and pH. *Langmuir,* 29(13)**,** pp 4350-6.

Betin, V. M., Singleton, B. K., Parsons, S. F., Anstee, D. J. & Lane, J. D. 2013. Autophagy facilitates organelle clearance during differentiation of human erythroblasts: evidence for a role for ATG4 paralogs during autophagosome maturation. *Autophagy,* 9(6)**,** pp 881-93.

Bhabra, G., Sood, A., Fisher, B., Cartwright, L., Saunders, M., Evans, W. H., . . . Case, C. P. 2009. Nanoparticles can cause DNA damage across a cellular barrier. *Nat Nano,* 4(12)**,** pp 876-883.

Blum, J. L., Xiong, J. Q., Hoffman, C. & Zelikoff, J. T. 2012. Cadmium associated with inhaled cadmium oxide nanoparticles impacts fetal and neonatal development and growth. *Toxicol Sci,* 126(2)**,** pp 478-86.

Bode, C. J., Jin, H., Rytting, E., Silverstein, P. S., Young, A. M. & Audus, K. L. 2006. In vitro models for studying trophoblast transcellular transport. *Methods Mol Med.,* 122(225-39.

Bramini, M., Ye, D., Hallerbach, A., Nic Raghnaill, M., Salvati, A., Aberg, C. & Dawson, K. A. 2014. Imaging approach to mechanistic study of nanoparticle interactions with the blood-brain barrier. *ACS Nano,* 8(5)**,** pp 4304-12.

Broad, K. D. & Keverne, E. B. 2011. Placental protection of the fetal brain during short-term food deprivation. *Proc Natl Acad Sci U S A,* 108(37)**,** pp 15237-41.

Campbell, I. L., Abraham, C. R., Masliah, E., Kemper, P., Inglis, J. D., Oldstone, M. B. & Mucke, L. 1993. Neurologic disease induced in transgenic mice by cerebral overexpression of interleukin 6. *Proc Natl Acad Sci U S A,* 90(21)**,** pp 10061-5.

Chen, Y., Vartiainen, N. E., Ying, W., Chan, P. H., Koistinaho, J. & Swanson, R. A. 2001. Astrocytes protect neurons from nitric oxide toxicity by a glutathione-dependent mechanism. *J Neurochem,* 77(6)**,** pp 1601-10.

Chen, Z. H., Wu, Y. F., Wang, P. L., Wu, Y. P., Li, Z. Y., Zhao, Y., . . . Shen, H. H. 2016. Autophagy is essential for ultrafine particle-induced inflammation and mucus hyperproduction in airway epithelium. *Autophagy,* 12(2)**,** pp 297-311.

Crighton, D., Wilkinson, S., O'Prey, J., Syed, N., Smith, P., Harrison, P. R., . . . Ryan, K. M. 2006. DRAM, a p53-induced modulator of autophagy, is critical for apoptosis. *Cell,* 126(1)**,** pp 121-34.

Danson, C. M., Pocha, S. M., Bloomberg, G. B. & Cory, G. O. 2007. Phosphorylation of WAVE2 by MAP kinases regulates persistent cell migration and polarity. *J Cell Sci,* 120(Pt 23)**,** pp 4144-54.

Dickey, J. S., Baird, B. J., Redon, C. E., Sokolov, M. V., Sedelnikova, O. A. & Bonner, W. M. 2009. Intercellular communication of cellular stress monitored by Œ≥-H2AX induction. *Carcinogenesis,* 30(10)**,** pp 1686-1695.

Dieriks, B., De Vos, W. H., Derradji, H., Baatout, S. & Van Oostveldt, P. 2010. Medium-mediated DNA repair response after ionizing radiation is correlated with the increase of specific cytokines in human fibroblasts. *Mutat Res,* 687(1-2)**,** pp 40-8.

Drogemuller, K., Helmuth, U., Brunn, A., Sakowicz-Burkiewicz, M., Gutmann, D. H., Mueller, W., . . . Schluter, D. 2008. Astrocyte gp130 expression is critical for the control of Toxoplasma encephalitis. *J Immunol,* 181(4)**,** pp 2683-93.

Fujita, N., Hayashi-Nishino, M., Fukumoto, H., Omori, H., Yamamoto, A., Noda, T. & Yoshimori, T. 2008. An Atg4B mutant hampers the lipidation of LC3 paralogues and causes defects in autophagosome closure. *Mol Biol Cell,* 19(11)**,** pp 4651-9.

Goeden, N., Velasquez, J., Arnold, K. A., Chan, Y., Lund, B. T., Anderson, G. M. & Bonnin, A. 2016. Maternal Inflammation Disrupts Fetal Neurodevelopment via Increased Placental Output of Serotonin to the Fetal Brain. *J Neurosci,* 36(22)**,** pp 6041-9.

Gonzalez-Perez, O., Gutierrez-Fernandez, F., Lopez-Virgen, V., Collas-Aguilar, J., Quinones-Hinojosa, A. & Garcia-Verdugo, J. M. 2012. Immunological regulation of neurogenic niches in the adult brain. *Neuroscience,* 226(270-81.

Grandjean, P. & Landrigan, P. J. 2014. Neurobehavioural effects of developmental toxicity. *Lancet Neurol,* 13(3)**,** pp 330-8.

Haroon, F., Drogemuller, K., Handel, U., Brunn, A., Reinhold, D., Nishanth, G., . . . Schluter, D. 2011. Gp130-dependent astrocytic survival is critical for the control of autoimmune central nervous system inflammation. *J Immunol,* 186(11)**,** pp 6521-31.

Hennessy, E., Griffin, E. W. & Cunningham, C. 2015. Astrocytes Are Primed by Chronic Neurodegeneration to Produce Exaggerated Chemokine and Cell Infiltration Responses to Acute Stimulation with the Cytokines IL-1beta and TNF-alpha. *J Neurosci,* 35(22)**,** pp 8411-22.

Hougaard, K. S., Jackson, P., Jensen, K. A., Sloth, J. J., Loschner, K., Larsen, E. H., . . . Vogel, U. 2010. Effects of prenatal exposure to surface-coated nanosized titanium dioxide (UV-Titan). A study in mice. *Part Fibre Toxicol,* 7(16.

Hung, T. H., Hsieh, T. T., Chen, S. F., Li, M. J. & Yeh, Y. L. 2013. Autophagy in the human placenta throughout gestation. *PLoS One,* 8(12)**,** pp e83475.

Hunter, C. A. & Jones, S. A. 2015. IL-6 as a keystone cytokine in health and disease. *Nat Immunol,* 16(5)**,** pp 448-57.

Klionsky, D. J., Abdelmohsen, K., Abe, A., Abedin, M. J., Abeliovich, H., Acevedo Arozena, A., . . . Zughaier, S. M. 2016. Guidelines for the use and interpretation of assays for monitoring autophagy (3rd edition). *Autophagy,* 12(1)**,** pp 1-222.

Li, H., van Ravenzwaay, B., Rietjens, I. M. & Louisse, J. 2013. Assessment of an in vitro transport model using BeWo b30 cells to predict placental transfer of compounds. *Arch Toxicol,* 87(9)**,** pp 1661-9.

Liddelow, S. A., Guttenplan, K. A., Clarke, L. E., Bennett, F. C., Bohlen, C. J., Schirmer, L., . . . Barres, B. A. 2017. Neurotoxic reactive astrocytes are induced by activated microglia. *Nature,* 541(7638)**,** pp 481-487.

Lock, R., Kenific, C. M., Leidal, A. M., Salas, E. & Debnath, J. 2014. Autophagy-dependent production of secreted factors facilitates oncogenic RAS-driven invasion. *Cancer Discov,* 4(4)**,** pp 466-79.

Ma, X., Wu, Y., Jin, S., Tian, Y., Zhang, X., Zhao, Y., . . . Liang, X. J. 2011. Gold nanoparticles induce autophagosome accumulation through size-dependent nanoparticle uptake and lysosome impairment. *ACS Nano,* 5(11)**,** pp 8629-39.

Mauer, J., Denson, J. L. & Bruning, J. C. 2015. Versatile functions for IL-6 in metabolism and cancer. *Trends Immunol,* 36(2)**,** pp 92-101.

Maycotte, P., Jones, K. L., Goodall, M. L., Thorburn, J. & Thorburn, A. 2015. Autophagy Supports Breast Cancer Stem Cell Maintenance by Regulating IL6 Secretion. *Mol Cancer Res,* 13(4)**,** pp 651-8.

Mohammadipour, A., Fazel, A., Haghir, H., Motejaded, F., Rafatpanah, H., Zabihi, H., . . . Bideskan, A. E. 2014. Maternal exposure to titanium dioxide nanoparticles during pregnancy; impaired memory and decreased hippocampal cell proliferation in rat offspring. *Environ Toxicol Pharmacol,* 37(2)**,** pp 617-25.

Muller, C. L., Anacker, A. M. J., Rogers, T. D., Goeden, N., Keller, E. H., Forsberg, C. G., . . . Veenstra-VanderWeele, J. 2017. Impact of Maternal Serotonin Transporter Genotype on Placental Serotonin, Fetal Forebrain Serotonin, and Neurodevelopment. *Neuropsychopharmacology,* 42(2)**,** pp 427-436.

Narita, M., Young, A. R., Arakawa, S., Samarajiwa, S. A., Nakashima, T., Yoshida, S., . . . Narita, M. 2011. Spatial coupling of mTOR and autophagy augments secretory phenotypes. *Science,* 332(6032)**,** pp 966-70.

Ostenfeld, T. & Svendsen, C. N. 2003. Recent advances in stem cell neurobiology. *Adv Tech Stand Neurosurg,* 28(3-89.

Pal, R., Mamidi, M. K., Das, A. K. & Bhonde, R. 2011. Human embryonic stem cell proliferation and differentiation as parameters to evaluate developmental toxicity. *J Cell Physiol,* 226(6)**,** pp 1583-95.

Papageorgiou, I., Brown, C., Schins, R., Singh, S., Newson, R., Davis, S., . . . Case, C. P. 2007. The effect of nano- and micron-sized particles of cobalt-chromium alloy on human fibroblasts in vitro. *Biomaterials,* 28(19)**,** pp 2946-2958.

Parry, M. C., Bhabra, G., Sood, A., Machado, F., Cartwright, L., Saunders, M., . . . Case, C. P. 2010. Thresholds for indirect DNA damage across cellular barriers for orthopaedic biomaterials. *Biomaterials,* 31(16)**,** pp 4477-4483.

Paull, T. T., Rogakou, E. P., Yamazaki, V., Kirchgessner, C. U., Gellert, M. & Bonner, W. M. 2000. A critical role for histone H2AX in recruitment of repair factors to nuclear foci after DNA damage. *Curr Biol,* 10(15)**,** pp 886-95.

Pevny, L. H., Sockanathan, S., Placzek, M. & Lovell-Badge, R. 1998. A role for SOX1 in neural determination. *Development,* 125(10)**,** pp 1967-78.

Polyzois, I., Nikolopoulos, D., Michos, I., Patsouris, E. & Theocharis, S. 2012. Local and systemic toxicity of nanoscale debris particles in total hip arthroplasty. *J Appl Toxicol,* 32(4)**,** pp 255-69.

Rothaug, M., Becker-Pauly, C. & Rose-John, S. 2016. The role of interleukin-6 signaling in nervous tissue. *Biochim Biophys Acta,* 1863(6 Pt A)**,** pp 1218-27.

Saei, A. A., Yazdani, M., Lohse, S. E., Bakhtiary, Z., Serpooshan, V., Ghavami, M., . . . Mahmoudi, M. 2017. Nanoparticle Surface Functionality Dictates Cellular and Systemic Toxicity. *Chemistry of Materials,* 29(16)**,** pp 6578-6595.

Shimizu, M., Tainaka, H., Oba, T., Mizuo, K., Umezawa, M. & Takeda, K. 2009. Maternal exposure to nanoparticulate titanium dioxide during the prenatal period alters gene expression related to brain development in the mouse. *Part Fibre Toxicol,* 6(20.

Shinozaki, Y., Shibata, K., Yoshida, K., Shigetomi, E., Gachet, C., Ikenaka, K., . . . Koizumi, S. 2017. Transformation of Astrocytes to a Neuroprotective Phenotype by Microglia via P2Y1 Receptor Downregulation. *Cell Rep,* 19(6), pp 1151-1164.

Simmons, D. G., Natale, D. R., Begay, V., Hughes, M., Leutz, A. & Cross, J. C. 2008. Early patterning of the chorion leads to the trilaminar trophoblast cell structure in the placental labyrinth. *Development,* 135(12), pp 2083-91.

Sofroniew, M. V. 2014. Multiple roles for astrocytes as effectors of cytokines and inflammatory mediators. *Neuroscientist,* 20(2), pp 160-72.

Sood, A., Salih, S., Roh, D., Lacharme-Lora, L., Parry, M., Hardiman, B., . . . Case, C. P. 2011. Signalling of DNA damage and cytokines across cell barriers exposed to nanoparticles depends on barrier thickness. *Nat Nanotechnol,* 6(12), pp 824-33.

Stern, S. T., Adiseshaiah, P. P. & Crist, R. M. 2012. Autophagy and lysosomal dysfunction as emerging mechanisms of nanomaterial toxicity. *Part Fibre Toxicol,* 9(20.

Sun, W., McConnell, E., Pare, J. F., Xu, Q., Chen, M., Peng, W., . . . Nedergaard, M. 2013. Glutamate-dependent neuroglial calcium signaling differs between young and adult brain. *Science,* 339(6116), pp 197-200.

Svendsen, C. N., ter Borg, M. G., Armstrong, R. J., Rosser, A. E., Chandran, S., Ostenfeld, T. & Caldwell, M. A. 1998. A new method for the rapid and long term growth of human neural precursor cells. *J Neurosci Methods,* 85(2), pp 141-52.

Takeda, K., Suzuki, K. I., Ishihara, A., Kubo-Irie, M., Fujimoto, R., Tabata, M., . . . Sugamata, M. 2009. Nanoparticles Transferred from Pregnant Mice to Their Offspring Can Damage the Genital and Cranial Nerve Systems. *J of Health Science,* 55(1), pp 95-102.

Thubagere, A. & Reinhard, B. M. 2010. Nanoparticle-induced apoptosis propagates through hydrogen-peroxide-mediated bystander killing: insights from a human intestinal epithelium in vitro model. *ACS Nano,* 4(7), pp 3611-22.

Yamashita, K., Yoshioka, Y., Higashisaka, K., Mimura, K., Morishita, Y., Nozaki, M., . . . Tsutsumi, Y. 2011. Silica and titanium dioxide nanoparticles cause pregnancy complications in mice. *Nat Nanotechnol.,* 6(5), pp 321-8. Epub 2011 Apr 3.

Zamanian, J. L., Xu, L., Foo, L. C., Nouri, N., Zhou, L., Giffard, R. G. & Barres, B. A. 2012. Genomic analysis of reactive astrogliosis. *J Neurosci,* 32(18), pp 6391-410.

Zhang, Y., Sloan, S. A., Clarke, L. E., Caneda, C., Plaza, C. A., Blumenthal, P. D., . . . Barres, B. A. 2016. Purification and Characterization of Progenitor and Mature Human Astrocytes Reveals Transcriptional and Functional Differences with Mouse. *Neuron,* 89(1)**,** pp 37-53.

Author Contributions

SJH, PC and MAC conceived and designed the experiments and CPC and MAC directed the work. SJH completed the experiments with the help of LAC, OC, PS, NJM, SFM and AS and also completed the data analysis with the help of MAC. JDL oversaw the autophagy experiments and the lentiviral shRNA experiments, and MS provided advice on the BeWo barriers. SK performed the in vivo injections and analysis was completed by AB, NB and AMM. SJH, CPC and MAC wrote the paper and all authors commented on it and agreed the final version.

Competing Financial Interests Statement

The authors declare no competing financial interests.

Additional information
Supplementary Information is available in the online version of the paper.

Reprints and permissions information is available at www.nature.com/reprints.

Correspondence and requests for materials should be addressed to MAC.
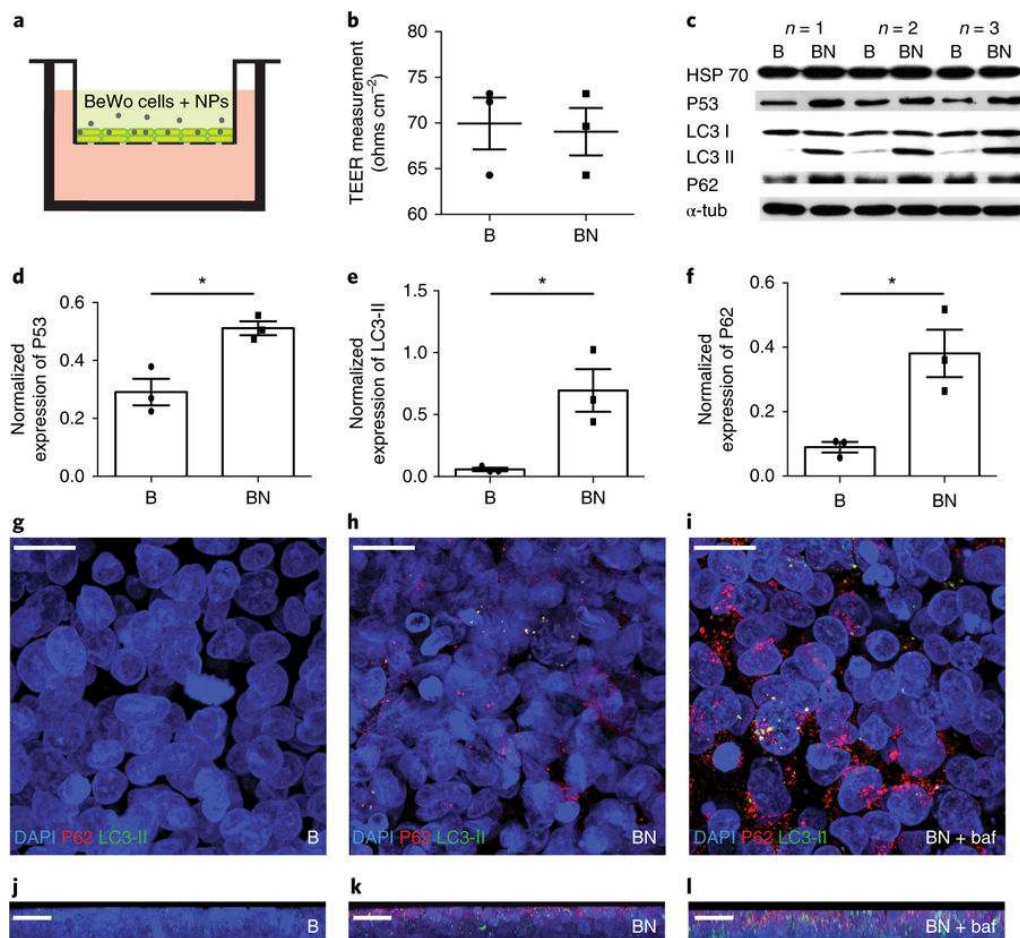
Figure 1: NPs alter autophagic flux in the upper layers of the BeWo barrier.

(a) BeWo barrier schematic. In the apical chamber BeWo cells are cultured on a transwell insert. NPs are then added apically, and the barrier assessed for autophagy markers 24 hours later (b) Mean TEER values of BeWo barriers demonstrating that TEER measurements are not affected by NP exposure. P = 0.2120; unpaired t-test, two-tailed (c) Immunoblots demonstrating the expression of stress induced autophagy markers (P53; LC3; P62), following NP exposure. n = 3 independent experiments. d-f, Normalised protein expression of: (d) P53, (e) lipidated LC3-II, (f) P62 All values are means + SEM from three independent experiments. Unpaired t-test, two-tailed. P values are = 0.0131 (d), 0.0209 (e) and 0.0183 (f). (g–l) Confocal immunocytochemistry for autophagy markers demonstrating increased LC3-positive puncta and staining intensity of P62 following exposure to NPs. (g-i) Upper layer of BeWo barrier (j-l) cross sectional images with the NP contact layer uppermost. B = barrier control, BN = barrier & NPs, BN+baf = BN & bafilomycin A1. Representative images from three independent experiments. Scale bars represent 30 μm.
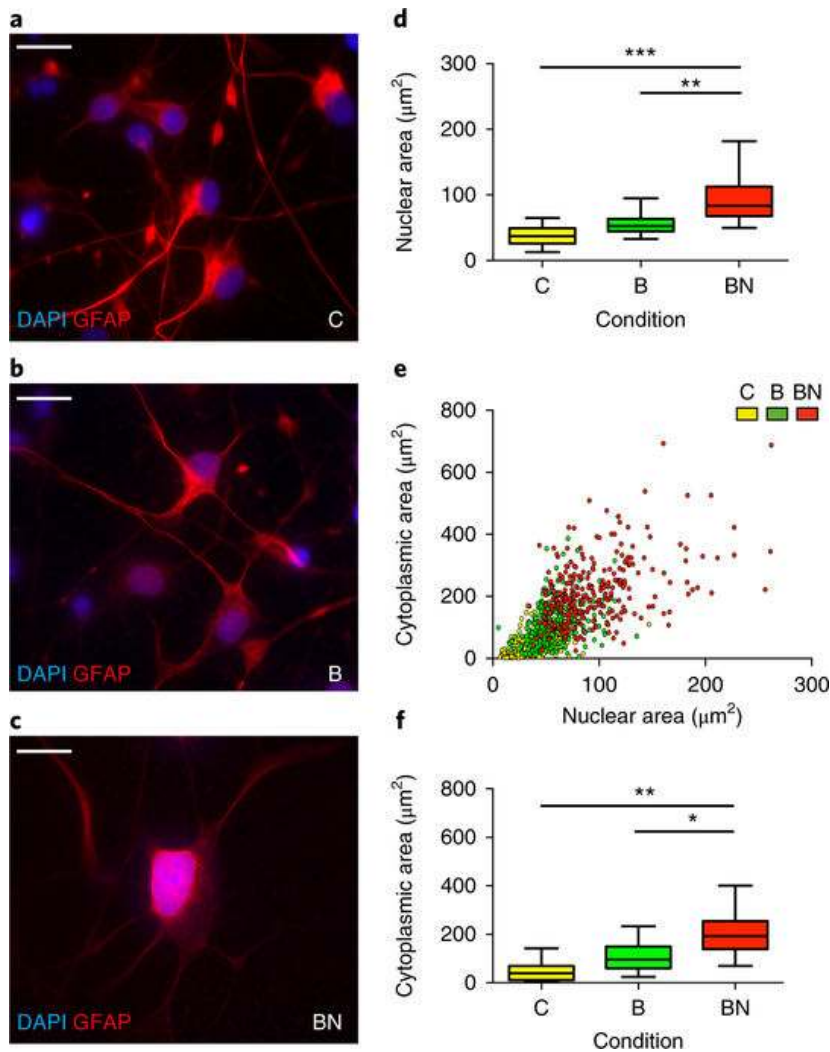
Figure 2: Astrocytes in mixed NPC culture undergo morphological changes following indirect exposure to NPs. (a-c) Representative images from three independent experiments showing immunostaining of GFAP in astrocytes for control (C), barrier (B) and barrier plus NPs (BN). Scale bars = 20 µm. (d-f) Plots showing astrocyte morphology in each condition (d, nuclear area, e, nuclear versus cytoplamic area, f, cytoplasmic area). d & f, 5th to 95th percentile box and whisker plots, and individual data outliers, showing astrocyte nuclear and cytoplasmic areas with statistical analysis performed on the means from three independent experiments by one way ANOVA, with Newman Keuls post hoc test. (d. F=29, P =0.0008, f. F=25 P=0.0013). e, Scatter plot showing all data points
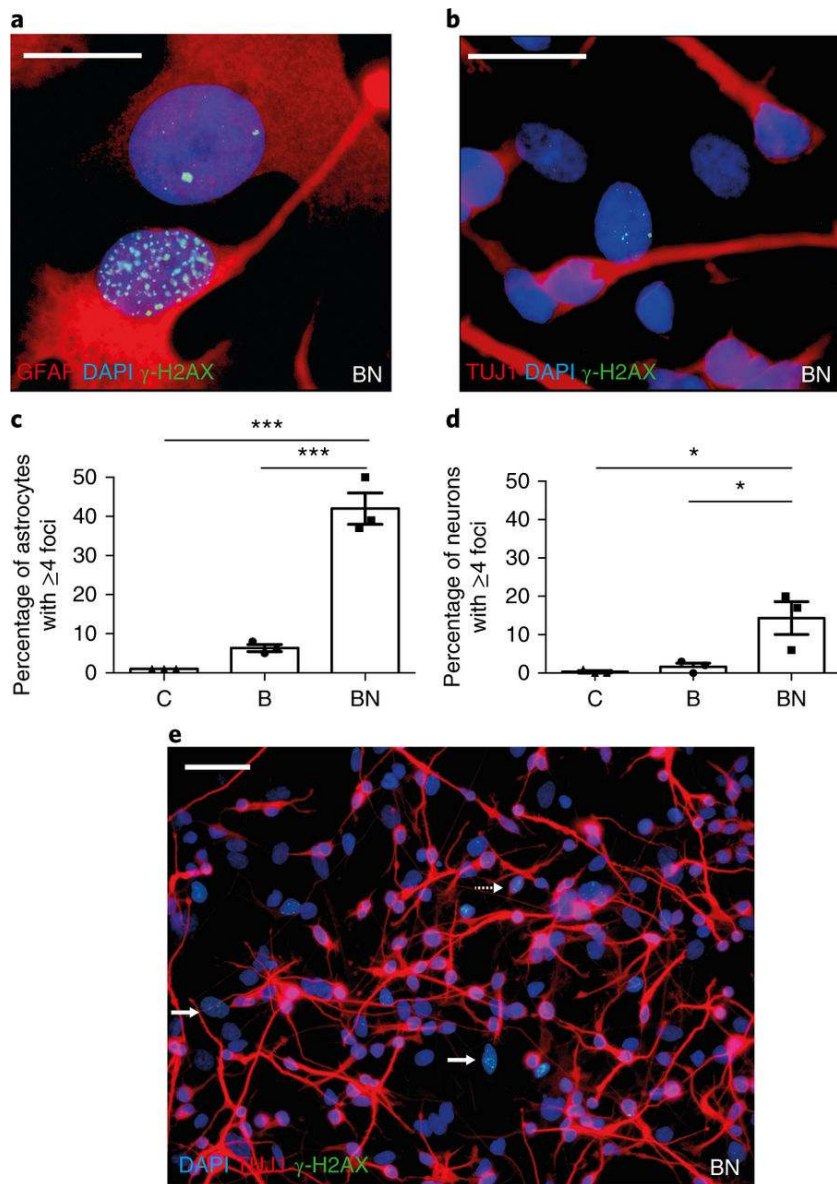
Figure 3: NPs increase the number of γ-H2AX foci in mixed astrocyte and neuronal cultures.

Immunostaining for γ-H2AX with: (a) GFAP+ve astrocytes and (b) TUJ1+ve neurons, scale bar = 10 μm. Representative images from three independent experiments. Graphs showing the percentage of: (c) astrocytes (P < 0.001 C vs BN and P = 0.001 B vs BN) and (d) neurons (P = 0.035 C vs BN and P = 0.0230 B vs BN) that contain ≥ 4 foci. All values are: means ± SEM from three independent experiments. One Way ANOVA, with Newman Keuls post hoc test. (e) Immunocytochemistry for γ-H2AX foci in differentiated NPCs with neurons identified using TUJ1. Representative image from three independent experiments. Dashed arrow indicates a neuron with

γ-H2AX foci while solid arrows show cells not immunostained for TUJ1 have increased levels of γ-

H2AX foci. Scale bar = 50 μm.
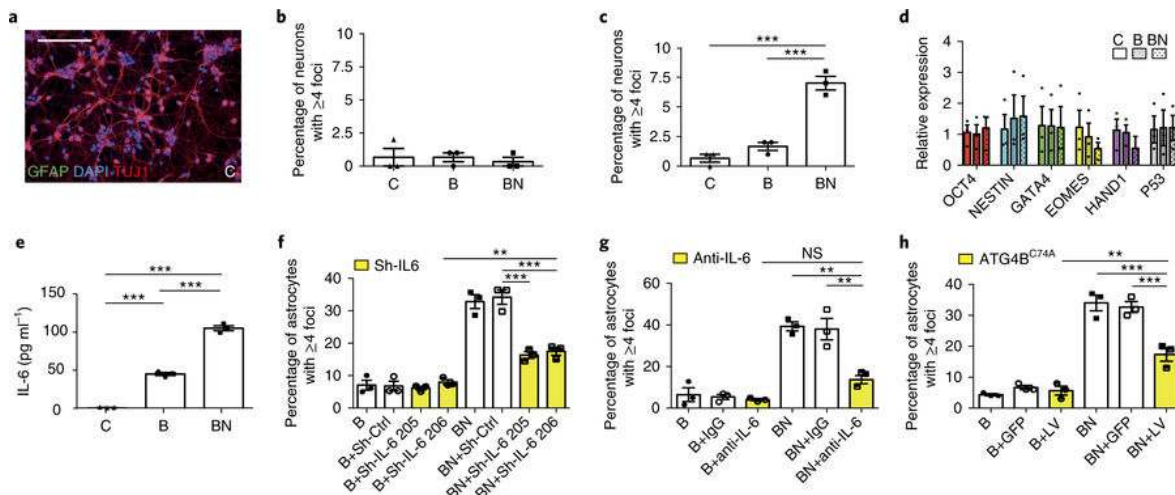
Figure 4: Mechanism of NP induced indirect toxicity is dependent on the presence of astrocytes and is triggered by autophagy in the BeWo barrier.

(a) Immunocytochemistry of primary neuronal cultures for GFAP and TUJ1 showing near pure TUJ1+ve neuronal cultures are formed from dissociated fetal tissue. Representative image from three independent experiments. Scale bar = 100 μm. (b) Graph of the number of γ-H2AX foci in primary neuron cultures. One way ANOVA, F= 0.2, P = 0.85. (c) γ-H2AX foci in primary neuronal cultures exposed to media conditioned on astrocytes One way ANOVA F= 63, P = 0.0001. Neumann Keuls post hoc P = 0.0001 C vs BN and P = 0.0003 B vs BN. (d) Indirect NP toxicity does not influence the formation of neuroectoderm during the differentiation of embryoid bodies. Samples were analyzed by qPCR, using 50ng of cDNA, for a panel of genes for regional identity. Data from three independent experiments was analysed by one way ANOVA: OCT4; F=0.1130, P = 0.8950; NESTIN F= 0.1232, P = 0.8862; GATA4 F= 0.0030, P = 0.9970; EOMES F= 0.6549, P = 0.5530; HAND1 F= 0.9105, P = 0.4515; P53, F= 0.0044, P = 0.9956. (e) Levels of IL-6 are increased in cultures of NPC derived astrocytes following exposure to NP conditioned media from the BeWo barrier. Data from three independent experiments was analysed by one way ANOVA: F= 566.1, P <0.0001. Neumann Keuls post hoc P < 0.0001 C vs N and C vs BN; P = 0.001 C vs B and B vs BN. (f) shRNA knock down of IL-6 production by the BeWo barrier significantly reduces the number of γ-H2AX foci in astrocytes. Data from three independent experiments was analysed by one way ANOVA: F=62.27; ***P< 0.0001. Neumann Kuels post hoc P < 0.0001 BN and BN+Sh

26

Ctrl vs BN+Sh-IL-6 205 and BN+Sh-IL-6 206. ** P = 0.0055 BN+Sh-IL-6-206 versus B+SH-IL-6

206 (g) Anti-IL-6 antibody blockade in conditioned media significantly reduces the number of γ-

H2AX foci in astrocytes, while relevant IgG had no effect. Data from three independent

experiments was analysed by one way ANOVA: F= 33.99. P<0.0001.

Neuman Keuls post hoc P=0.0004 BN vs BN+anti-IL-6 and P=0.0006 BN+IgG vs BN+anti-IL-6 (h)

Autophagy inhibition in BeWo cells exposed to NPs reduces the number of γ-H2AX foci in

astrocytes in mixed cultures.
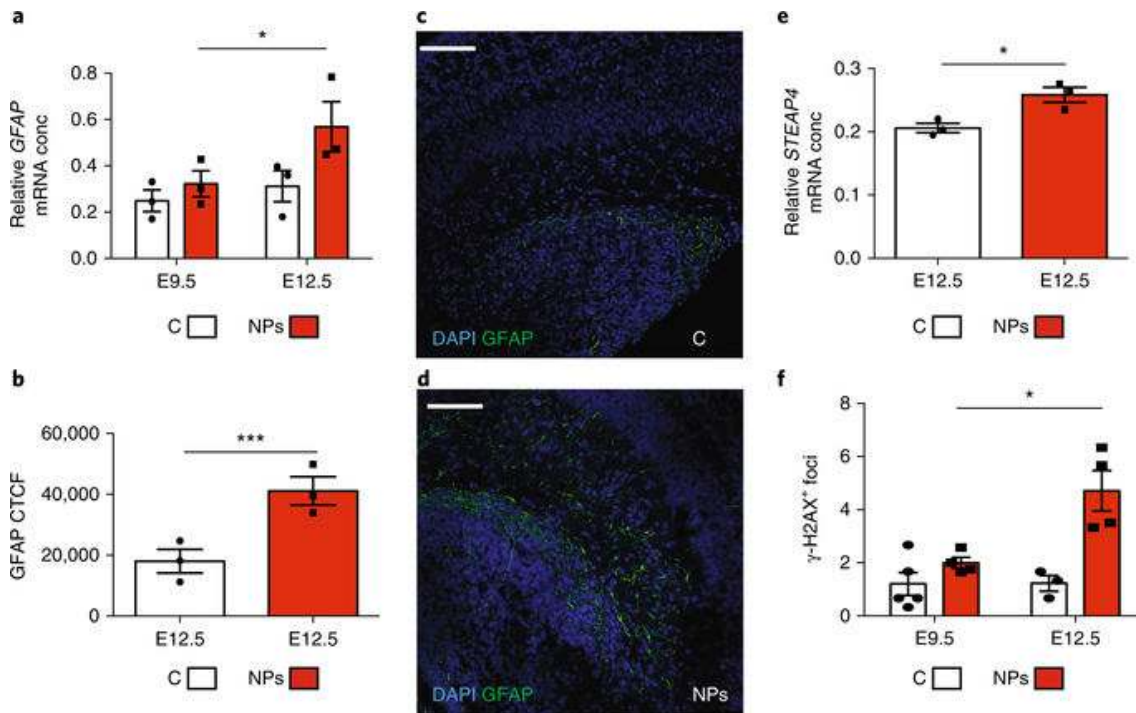
Figure 5. GFAP and γ-H2AX levels are increased in the hippocampus of neonates following maternal exposure to CoCr NPs at E12.5.

(a) *GFAP* gene expression is increased the brains of neonates following maternal CoCr NP administration at E12.5 but not at E9.5. Data from three independent animals was analysed by 2-way ANOVA, CoCr treatment effect F=6.120; P=0.03 and age effect F=5.409; P=0.048. (b) quantification of GFAP using corrected total cell fluorescence (CTCF) demonstrates greater GFAP expression in the hippocampus following NPs exposure at E12.5. P= 0.0191; unpaired t-test, two tailed (c) immunocytochemistry image of the hippocampus of saline control showing negligible GFAP staining. (d) immunocytochemistry image of the hippocampus in NP exposed group at E12.5 showing increased GFAP staining. Representative images from three independent animals (Scale bars = 100 μm) (e) *STEAP4* gene expression is increased in the hippocampus following maternal exposure to NPs at E12.5. Data from three independent animals, P= 0.0206; unpaired t-test, two tailed (f) quantification of γ-H2AX in the hippocampus demonstrates a greater number of foci following exposure to NPs at E12.5. Data from three to five independent animals was analysed by 2-way ANOVA with Bonferroni post hoc: CoCr treatment effect F=14.13; P=0.0032 and age effect F=5.878; P=0.0337.

Nanoparticle induced neuronal toxicity across placental barriers is mediated by autophagy and dependent on astrocytes

Simon J Hawkins , Lucy A Crompton, Aman Sood, Margaret Saunders, Noreen Boyle, Amy

Buckley, Aedin M Minogue, Sarah F. McComish, Natalia Jimenez Moreno, Oscar Cordero-Llana,

Petros Stathakos, Stephen Kelly, Jon D Lane, C. Patrick Case, and Maeve A Caldwell.
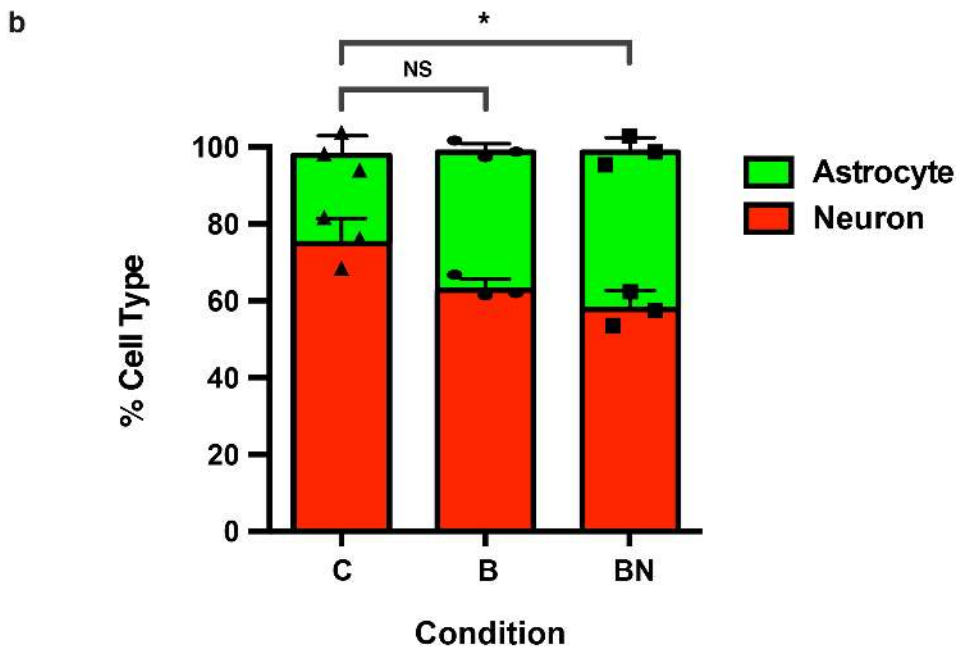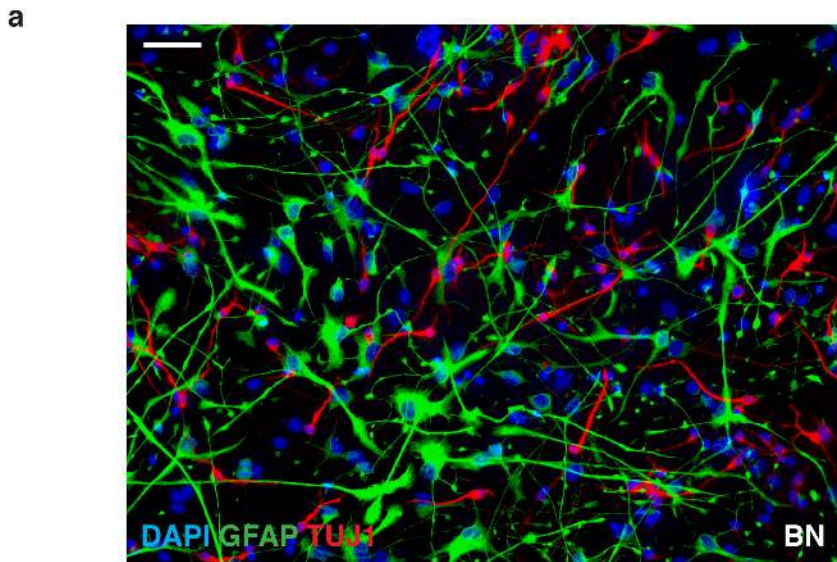
Supplementary Figures
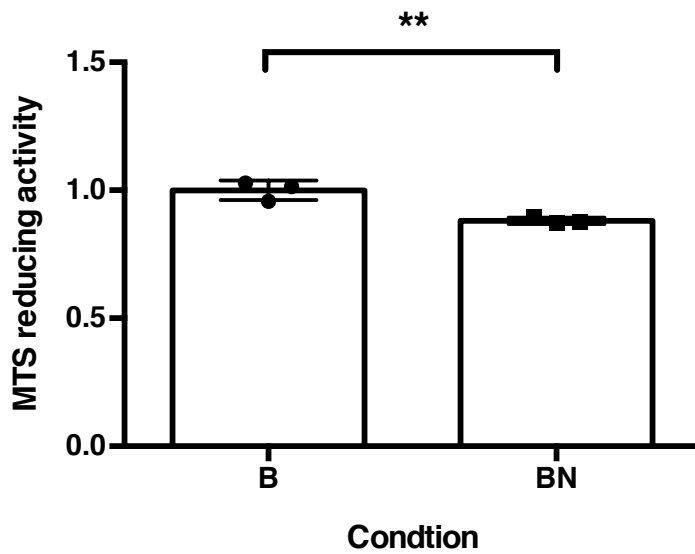
Supplementary Figure 1: Mitochondrial activity in the BeWo barrier following CoCr NP exposure. A decrease in MTS reducing activity was found following the exposure of BeWo barriers to CoCr NPs (BN) for 24 hours. Results are from three independent experiments and were analysed using an unpaired student's T test, two tailed. Data are normalised to the barrier only control (B). All values are: means ± sem from three independent experiments. ** $P = 0.0064$.
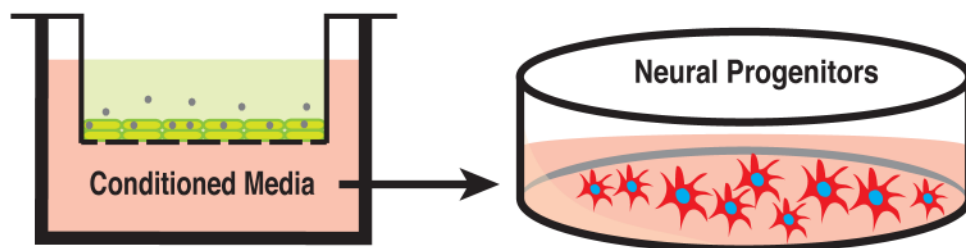
Supplementary Figure 2: BeWo barrier media transfer model with neural progenitor cells

BeWo cells, a human trophoblast choriocarcinoma derived cell line, were grown on transwell inserts for 7 days so as to form confluent bilayered cell barriers used to model the placental barrier in vitro (Figure 1a) (Bhabra et al., 2009; Sood et al., 2011; Parry et al., 2010; Bode et al., 2006). After 7 days the barriers were checked for barrier integrity, TEER measurements shown in (Figure 1b), then 0.04mg/ml of CoCr NPs were applied to the upper layer. Neural progenitor cell media was placed beneath the barrier in the lower chamber and conditioned for 24 hours. This was then placed onto the dissociated neural progenitor cells. These had been dissociated and allowed to commence differentiating for 24 hours prior to exposure. These cells were then cultured in the transferred media for 6 days before the differentiated neuroprogenitor cells were assessed.

Supplementary Figure 3: The proportion of neurons and astrocytes formed from dissociated NPCs following indirect exposure to CoCr NPs.
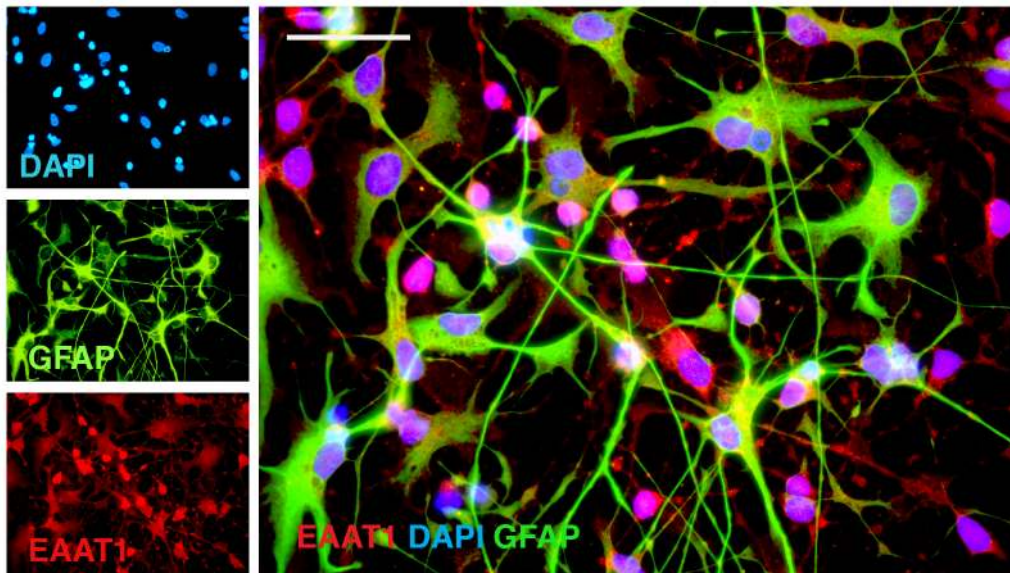
(a) Immunostaining of differentiated NPCs for GFAP and TUJ1 with scale bar 50 μm. Representative image from three independent experiments (b) Graph of cell counts for GFAP[+] astrocytes and TUJ1^{+} neurons showing no barrier control (C), Barrier only control (B) and Barrier with CoCr NP exposure (BN). All values are: means + SEM from three independent experiments. Statistical analysis compares percentage of neurons by one way ANOVA with Newman Keuls post hoc test. NS = P ≥ 0.05, C v BN P = 0.0426.
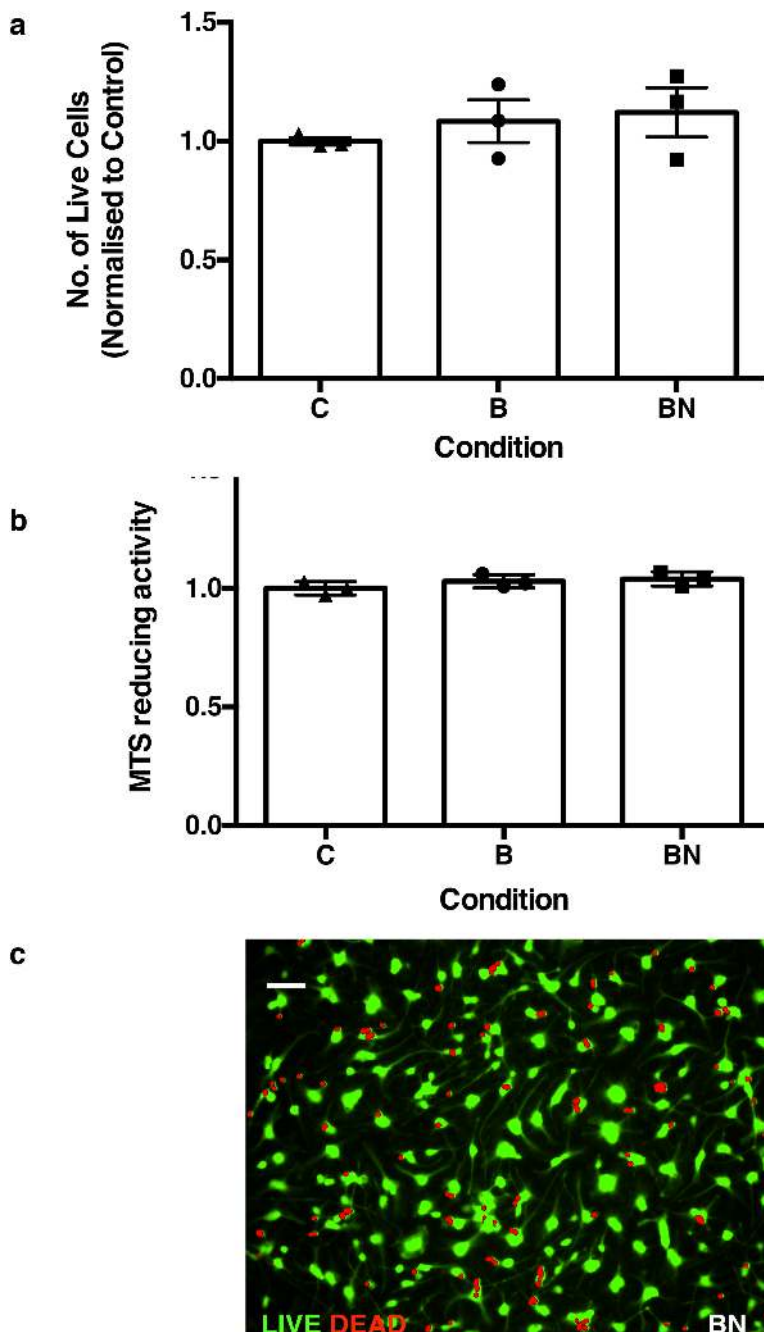
Supplementary Figure 4: Viability of neural progenitor cells following indirect exposure to CoCr NPs. (a) Graph of Live Dead cells counts across exposure conditions assessed on day 7 of differentiation demonstrating no difference was found. P=0.5751 (b) Graph of MTS reducing activity also showing no difference between conditions. P=0.2881 All values are: means ± sem from three independent experiments. Data is normalised to control and no significant difference was found on ANOVA. (c) Live Dead cell image of BN exposed NPCs. Representative image of three independent experiments yielding similar results. Scale bar 50 μm.

Supplementary Figure 5: Dissociated NPCs differentiate to form neurons and astrocytes.
Representative image of three independent experiments yielding similar results. These images demonstrate co-staining of GFAP^{+} cells with EAAT1. Scale bar is 50 µm.
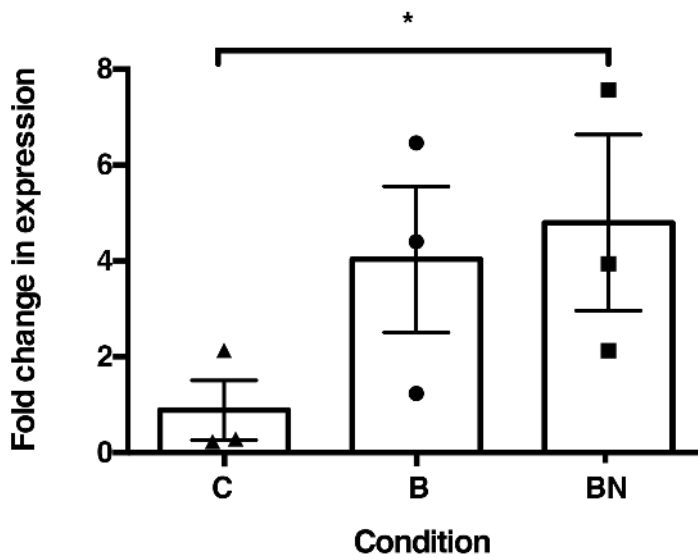
Supplementary Figure 6: Increased gene expression of *GFAP* did not occur in differentiated neuroprogenitors following CoCr NP exposure to the BeWo barrier.

Samples from differentiated neuroprogenitor cells were analyzed for *GFAP* expression by qPCR, using 50ng of cDNA. All values are: means ± sem from three independent experiments. *$P <$ 0.0408 by ANOVA and Newman Keuls post hoc test.
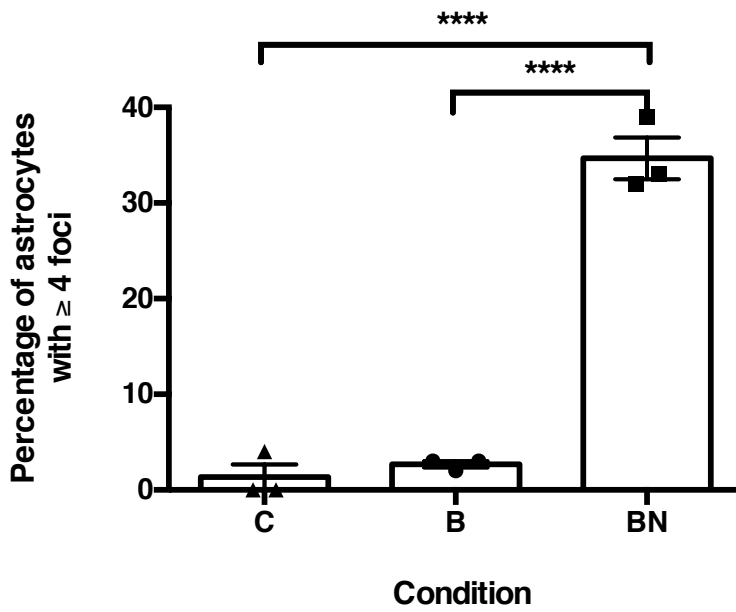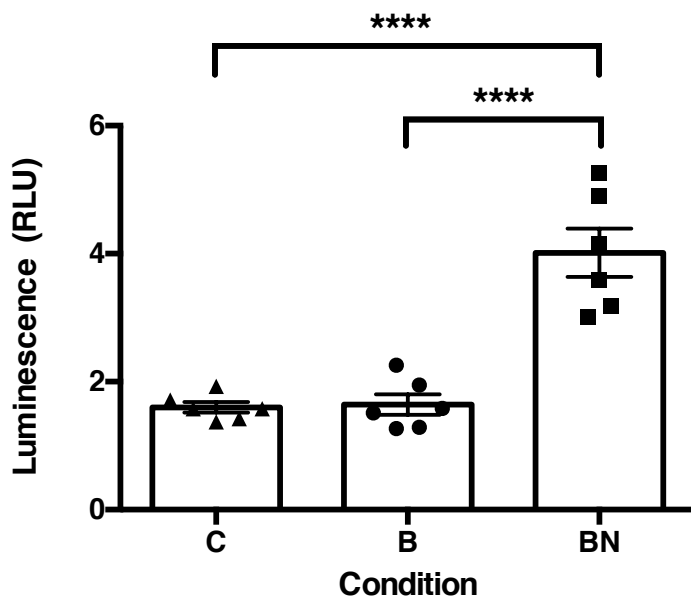
Supplementary Figure 7: TiO$_2$ NPs exposure to BeWo barriers results in an increase in the number of γ-H2AX foci in astrocytes.

Graph showing the percentage of astrocytes that contain ≥ 4 foci. All values are: means ± sem from three independent experiments. **** = P < 0.0001 by ANOVA and Newman Keuls post hoc test.
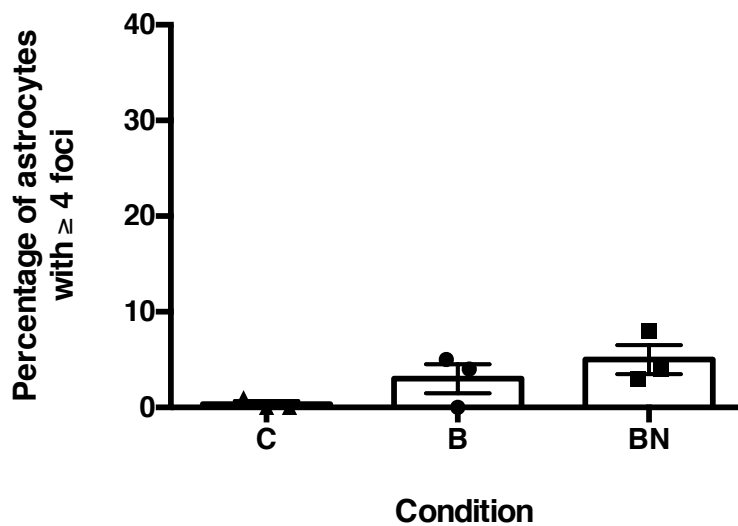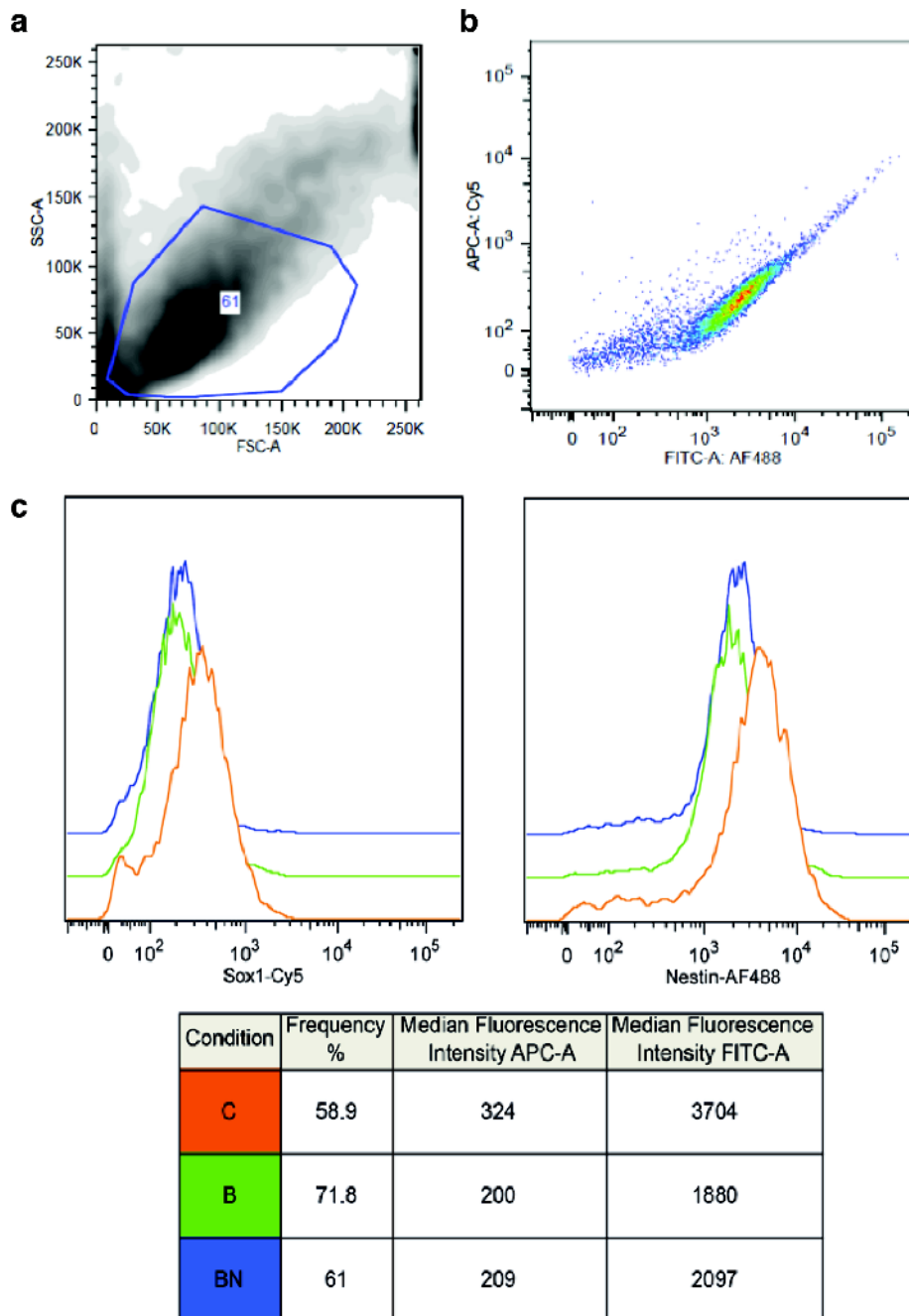
Supplementary Figure 8: F127 NP exposure to BeWo barriers does not result in an increase in the number of γ-H2AX foci in astrocytes.

Graph showing the percentage of astrocytes that contain ≥ 4 foci. All values are: means ± sem from three independent experiments. P = 0.1010; NS by ANOVA.

Supplementary Figure 9: Determination of glutathione levels in NPC cultures following indirect exposure to NPs. Graph of glutathione induced luminescence showing increased glutathione levels in NPCs differentiated in BN media. All values are: means ± sem from six independent experiments. **** = P < 0.0001 by ANOVA and Newman Keuls post hoc test.

| Condition	Frequency %	Median Fluorescence Intensity APC-A	Median Fluorescence Intensity FITC-A
C	58.9	324	3704
B	71.8	200	1880
BN	61	209	2097

Supplementary Figure 10: Flow cytometry assessment of NSC markers Nestin and Sox1 in exposed embryoid bodies.

(a) The gating strategy was forward and side scatter (using a gate that was applied to all samples), followed by (b) analysis of median fluorescence for AF488 Nestin (green) and Cy5 Sox1 (blue). (c) Indirect NP toxicity does not affect the formation of neuroectoderm during the differentiation of embryoid bodies. Data shown is from one representative experiment from three independent experiments.
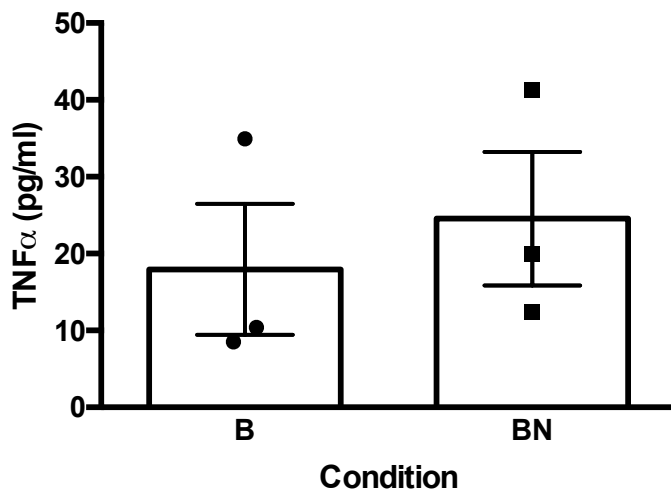
Supplementary Figure 11: TNFα levels in media conditioned beneath the BeWo Barrier

TNFα levels assessed by enzyme-linked immunosorbent assay found no increased expression

following CoCr NP exposure. All values are: means ± sem from three independent experiments. P

= 0.6163; NS by unpaired T test, two tailed.
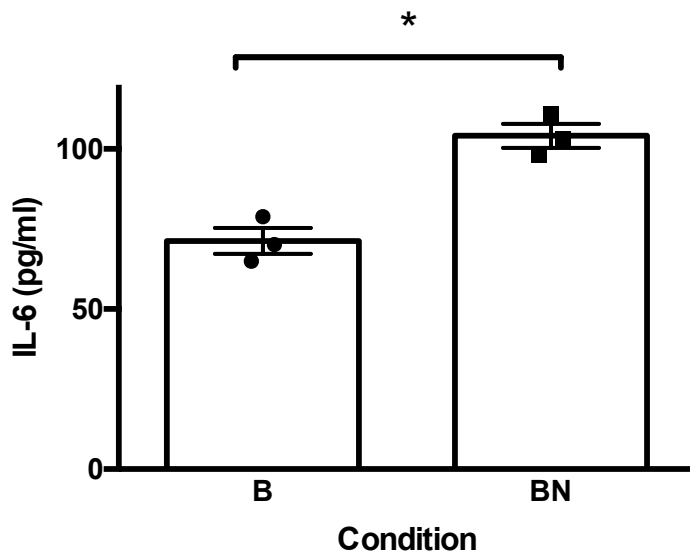
Supplementary Figure 12: IL-6 was released from BeWo barriers following the exposure of NPs.

IL-6 levels assessed by enzyme-linked immunosorbent assay were found to be significantly increased following CoCr NP exposure. All values are: means ± sem from three independent experiments. * P = 0.041 by unpaired T test, two tailed.
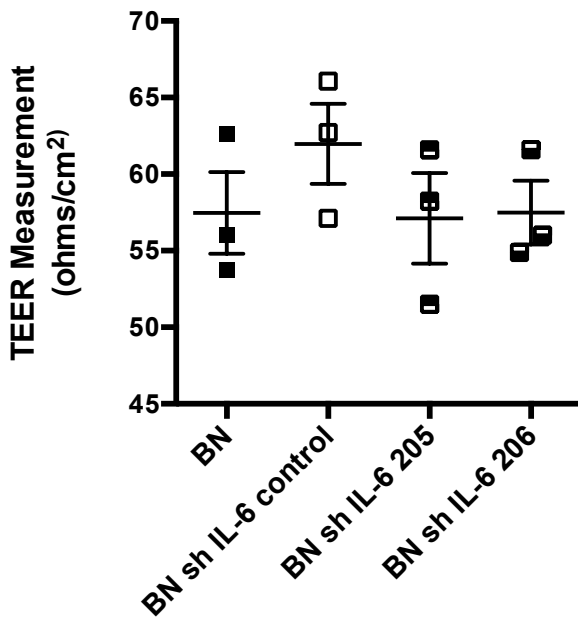
Supplementary Figure 13: TEER values of BeWo barriers following transduction of IL-6 sh-RNA using a lentiviral vector.

BeWo barriers were either transduced with shRNA lentiviral particles (or not transduced as a control). PLKO1 non-targeting shRNA (Sigma), or IL6 shRNAs TRCN0000059205 or TRCN0000059206 (Sigma), were added above and below the barrier BEWO media. TEER measurements were not found to be significantly altered following these exposures and similar TEER levels were achieved as in BeWo barriers not exposed to lentiviral vectors (See Figure 1b for comparison). All values are: means ± sem from three independent experiments. P=0.5320; NS by two way - ANOVA.
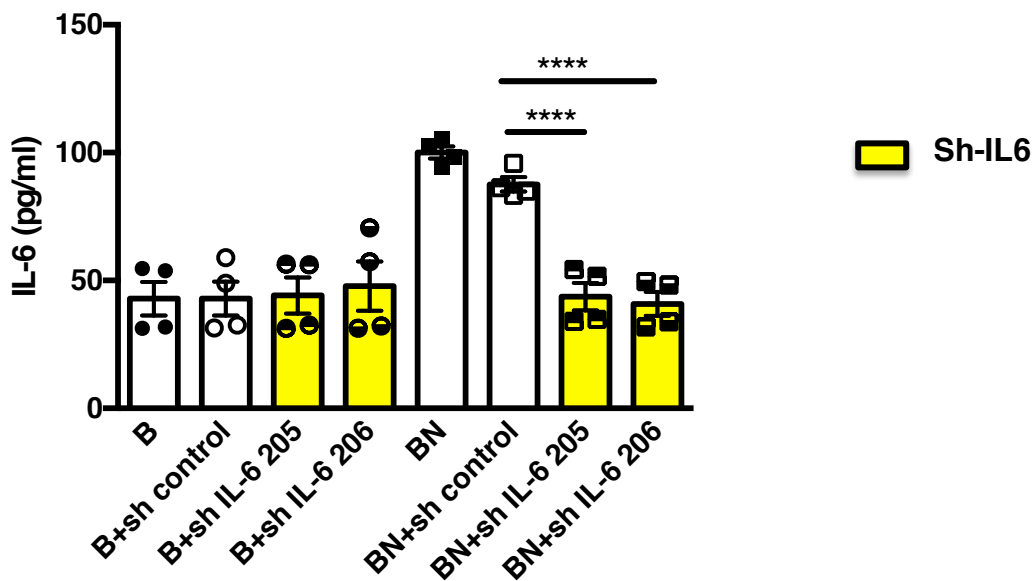
Supplementary Figure 14: Levels of IL-6 are increased following exposure of nanoparticles to the BeWo barrier, addition of an IL-6 shRNA reduces the level of IL-6 to control levels.
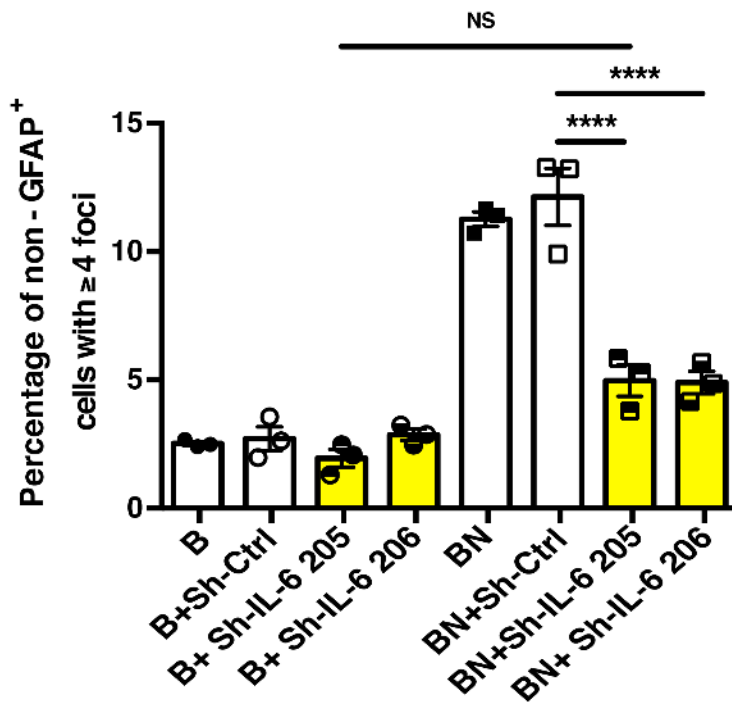
BeWo barriers were either transduced with shRNA lentiviral particles (or not transduced as a control). PLKO1 non-targeting shRNA (Sigma), or IL6 shRNAs TRCN0000059205 or TRCN0000059206 (Sigma), were added above and below the barrier BEWO media. Addition of an IL-6 shRNA reduces the level of IL-6; shRNA control has no effect (Data presented as mean + SEM of n=4 independent experiments). One way ANOVA plus Neuman Keuls post hoc test. **** $P < 0.0001$ BN and BN+Sh control vs BN+Sh IL-6 205 and BN+Sh IL-6 206. B is barrier only; BN is barrier with nanoparticles.

Supplementary Figure 15: Levels of γ-H2AX are increased in non-GFAP+ cells following exposure of nanoparticles to the BeWo barrier, then reduced to control levels following the addition of an IL-6 shRNA.

BeWo barriers were either transduced with shRNA lentiviral particles (or not transduced as a control). PLKO1 non-targeting shRNA (Sigma), or IL6 shRNAs TRCN0000059205 or TRCN0000059206 (Sigma), were added above and below the barrier BEWO media. This significantly reduced the number of γ-H2AX foci in non-GFAP positive cells; based on Suppl Figure 3 these are considered likely to be neurons (n=3). Data presented as mean + SEM of n=3 independent experiments). One way ANOVA plus Neuman Keuls post hoc test. **** P < 0.0001

BN and BN+Sh ctrl vs BN+Sh IL-6 205 and BN+Sh IL-6 206. B is barrier only; BN is barrier
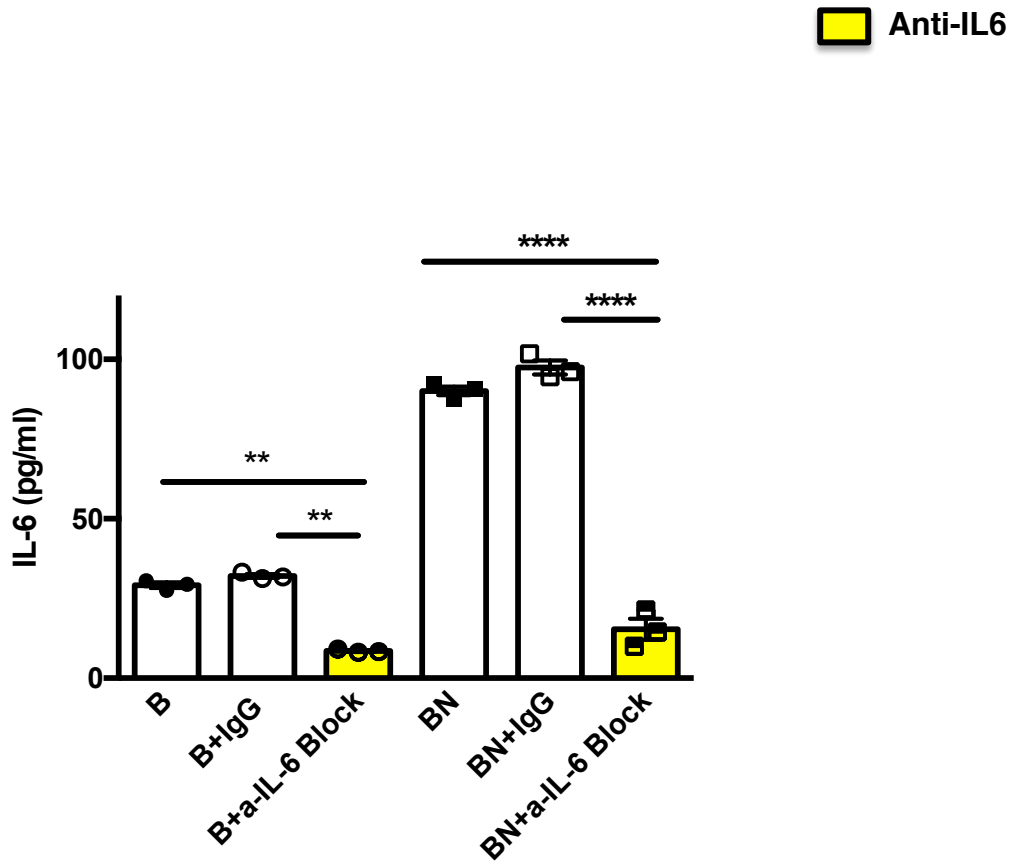
with nanoparticles.

Supplementary Figure 16. **Levels of IL-6 are increased following exposure of nanoparticles to the BeWo barrier, addition of an IL-6 blocking antibody reduces the level of IL-6**.

IgG control has no effect (n=3 independent experiments). Data presented as mean + SEM of n=3 independent experiments). One way ANOVA plus Neuman Keuls post hoc test. ** $P = 0.0040$ B vs B+a-IL-6 Block and $P = 0.0082$ B+IgG vs B+a-IL-6 Block. **** $P < 0.0001$ BN+a-IL-6 Block versus BN and BN + IgG control antibody. B is barrier only; BN is barrier with nanoparticles.
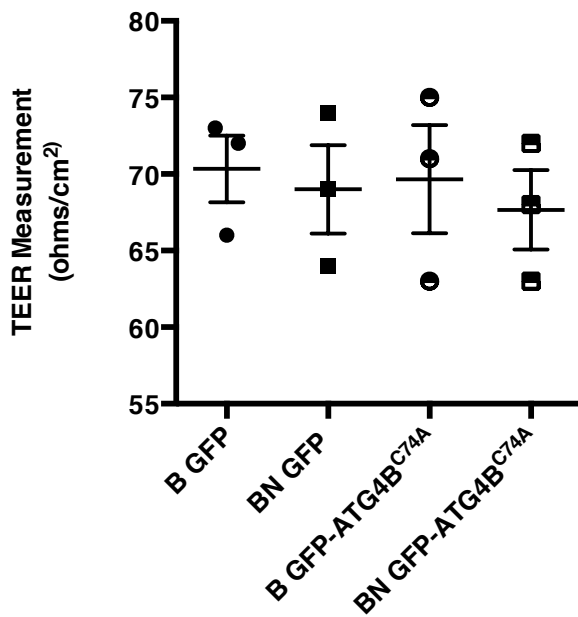
Supplementary Figure 17: TEER values of BeWo barriers following inhibition of autophagic degradation using a lentiviral vector containing human ATG4B^{C74A}

BeWo barriers were either transduced with lentiviral vectors containing GFP or GFP- ATG4B^{C74A}. These were then exposed to media containing CoCr NPs or media only. TEER measurements were not found to be significantly altered following these exposures and similar TEER levels were achieved as in BeWo barriers not exposed to lentiviral vectors (See Figure 1b for comparison). All values are: means ± sem from three independent experiments. P= 0.9761; NS by two way - ANOVA.
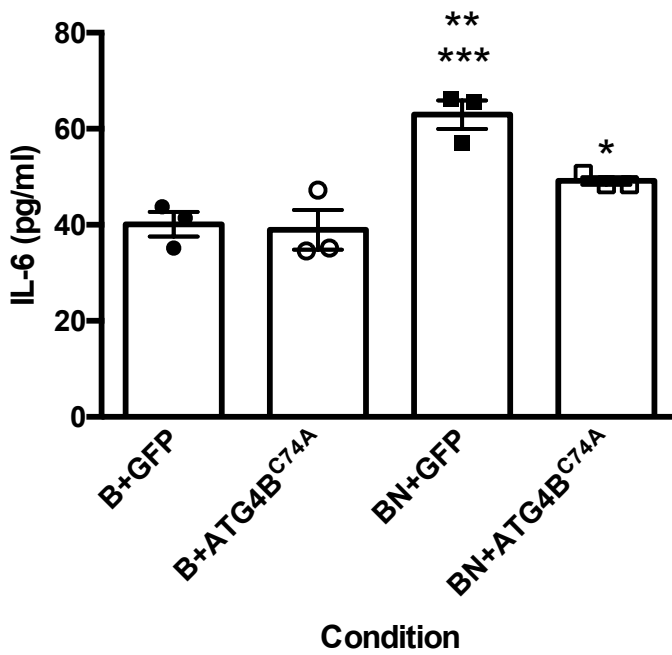
Supplementary Figure 18: IL-6 secretion from the BeWo barriers exposed to NPs in the presence of ATG4B^{C74A} released less IL-6 than control GFP-expressing barriers.

Measured by enzyme-linked immunosorbent assay. Means with SEM from three independent experiments assessed by One way ANOVA with Neuman Keuls post hoc test. Significance Values:

* P = 0.0370 versus BN+GFP; ** P = 0.0022 and *** P = 0.0001 versus B+GFP and B+ATG4B^{c74A}
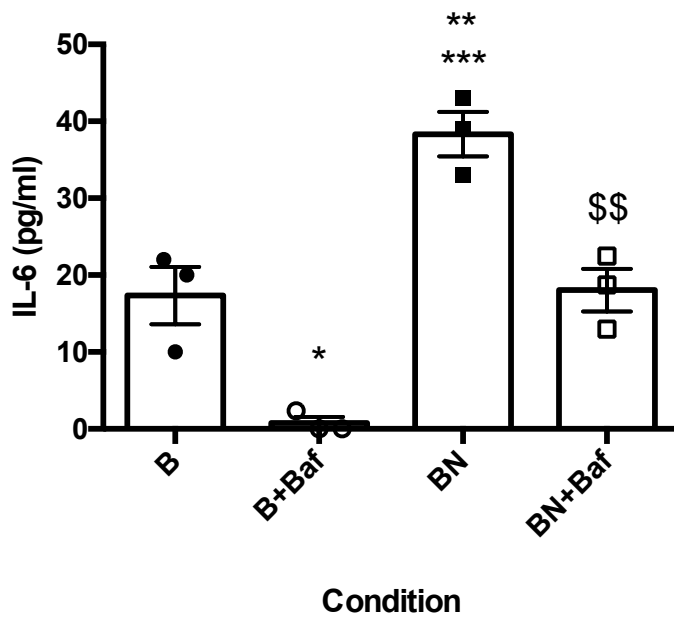
Supplementary Figure 19: IL-6 secretion from the BeWo barriers exposed to NPs in the presence of BafA1 also secreted significantly less IL-6 than barriers exposed to NPs in the absence of BafA1.

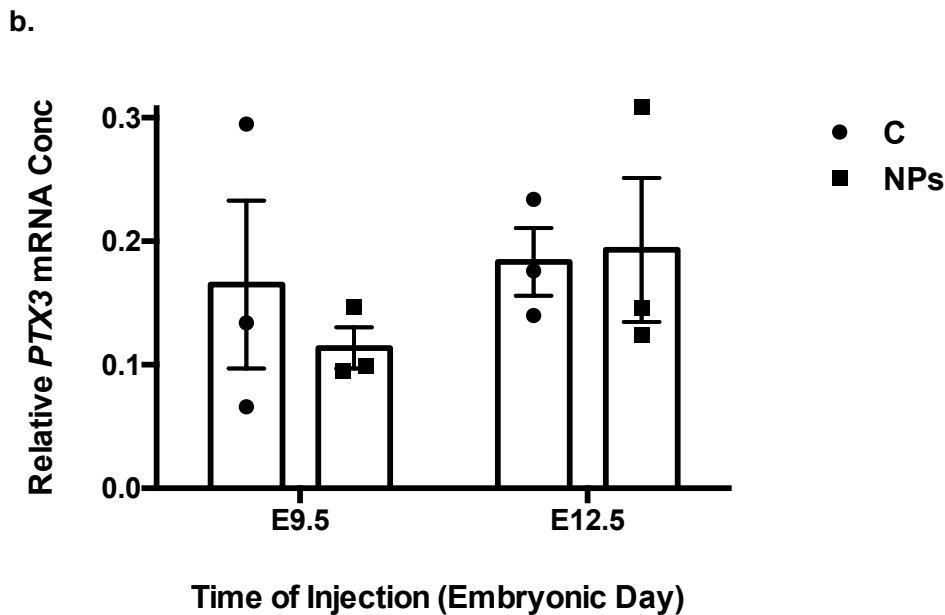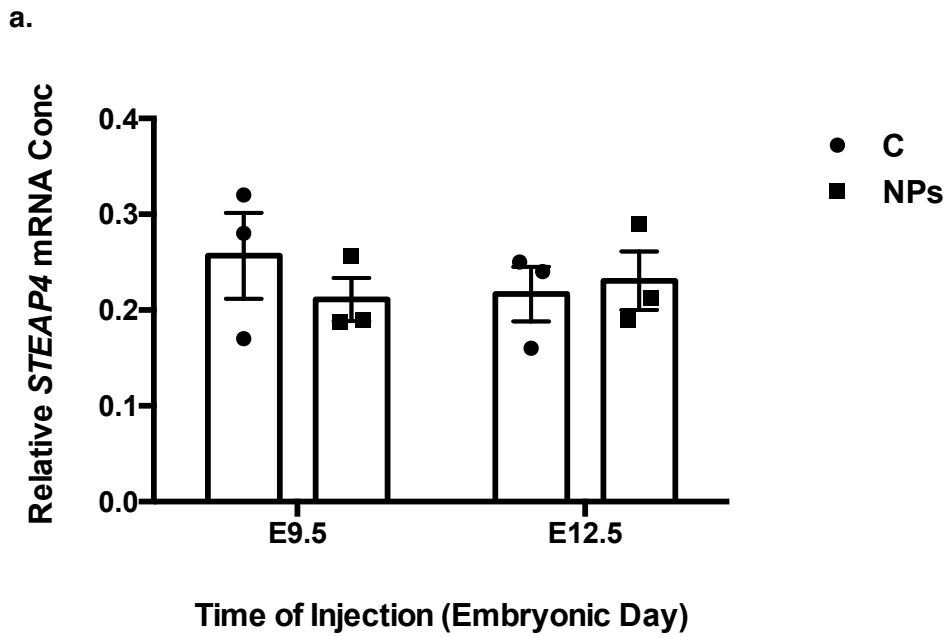Measured by enzyme-linked immunosorbent assay. Means with sem of three independent experiments assessed by One way ANOVA with Neuman Keuls post hoc test. Significance values: * P= 0.05 versus B; $$ P = 0.0058vs B+Baf and P = 0.0036 vs BN; ** P = 0.0036 versus B; *** P≤0.001 versus B+Baf.

a.

b.

Supplementary Figure 20: Expression of the astrocytic activation markers (a) *STEAP4* and (b) *PTX3* did not alter significantly at either time-point of NP exposure in whole brain when compared to relevant control groups.

Gene expression assessment performed by qPCR relative to GAPDH expression. All values are: means ± sem from three independent experiments. NS by Two way - ANOVA. (a) $P = 0.3345$ for CoCr treatment and $P = 0.6729$ for E9.5 vs E12.5; (b) $P = 0.7631$ for CoCr treatment and $P = 0.6402$ for E9.5 vs E12.5.
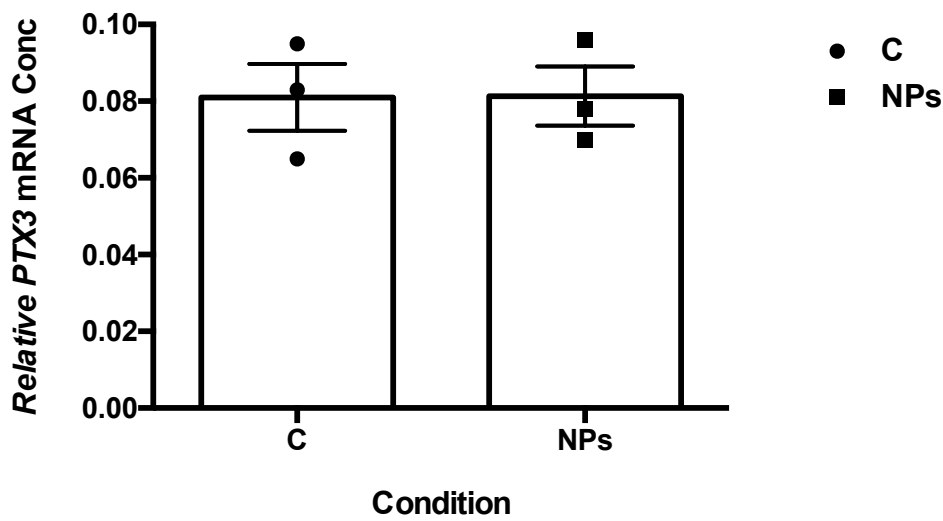
Supplementary Figure 21: Levels of PTX3 gene expression were not increased in the hippocampus following NP exposure at E12.5.

Gene expression assessment performed by qPCR. All values are: means ± sem from three independent experiments. P = 0.9785; NS by unpaired t test, two tailed.
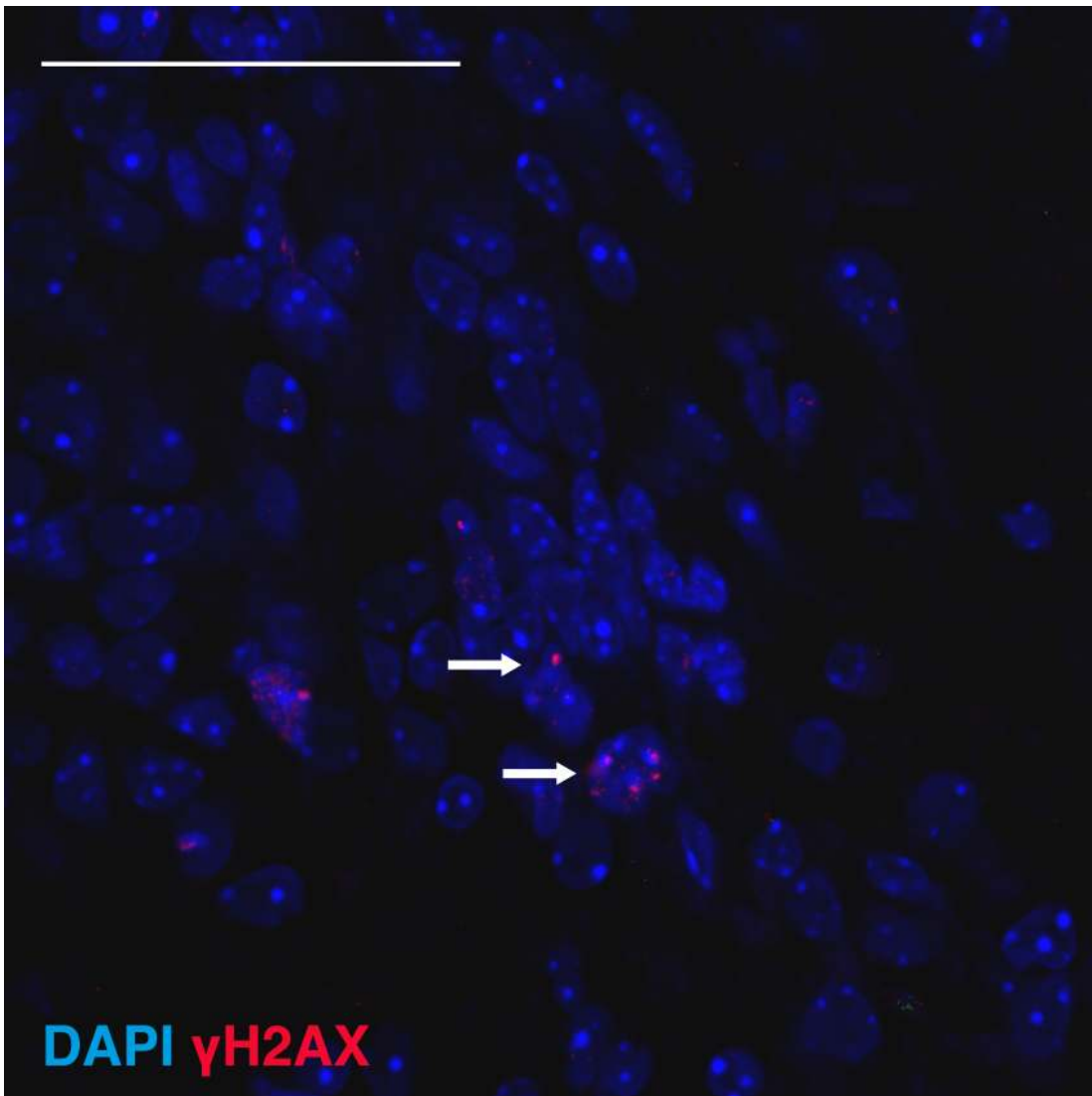
Supplementary Figure 22: Immunohistological staining for y-H2AX demonstrated significantly increased DNA damage in the hippocampus in E12.5 treated animals only compared to relevant controls

This demonstrate that increased y-H2AX immunostaining (white arrows) was present in the hippocampus of mice at E12.5 following maternal exposure to CoCr NPs. Representative image from four independent animals yielding similar results. Scale bar is 50 µm.

Supplementary methods

Preparation of nanoparticles

The 80 ± 14.6 nm CoCr NPs used were produced by a thermal plasma method (Raghunathan et al., 2013). They were polydisperse in size measuring 80 ± 14.6 nm with a smooth outline with some straight edges on transmission electron microscopy using a Jeol 1200EXmkII TEM operated at 120 keV. They had a mean electrophoretic mobility at 25oC of -0.816 μ o−1/Vcm−1 and a mean zeta potential of -13mv measured on Malvern Instruments Zetasizer Nano Z equipment. In media they have a tendency to aggregate demonstrated by a photon correlation spectroscopy measurement of 241nm in media carried out on a Brookhaven instrument and release predominantly Co ions (Raghunathan et al., 2013).

The NPs were prepared for use in tissue culture by being: placed in glass universals, weighed then washed with 100% ethanol. They were then heat sterilized at 180oC for 3 hours then resuspended in serum free growth media by sonication with 7 pulses each of 2 seconds long using a titanium probe and Sonics VibraCELL VC130PB sonicator (maximum output power: 130W). The metal NP exposures were expressed in mg/ml, this equates to 0.036 mg per cm^2 surface area of BeWo barrier. This was calculated from the mass of the NPs before addition of media in relation to the surface area of the Transwell insert on which the BeWo cells were grown. The surface area of the Transwell insert used in all the experiments was 1.12 cm^2.This exposure level has previously been found not to cause transition of CoCr NPs across the BeWo barrier (Bhabra et al., 2009; Parry et al., 2010; Sood et al., 2011).

TiO2 NPs used for comparison to CoCr NPs were 50 nm ± 20 nm (Sood et al., 2011). 5% F127 NPs were kindly donated by Dr Bienemann from the University of Bristol and setup as previously described (Basak and Bandyopadhyay, 2013; Liu et al., 2016).

Supplementary Table 1: Composition of CoCr alloy (Raghunathan et al., 2013).

Element	C	Co	Cr	Fe	Mn	Mo	N	Ni	Si
Wt%	0.06	64.3	28.0	0.25	0.50	6.00	0.20	0.20	0.50
Atomic%	0.29	62.5	30.8	0.26	0.52	3.58	0.82	0.20	1.02

Transduction of BeWo barriers with IL-6 sh-RNA lentivirus.

Bewo cells were grown on transwell inserts for 7 days to form confluent bilayered layers of the cells. They were seeded at 10^5 cells/cm^2 on transwell inserts (Appleton Woods, Birmingham, UK) in Dulbecco's Modified Eagle's Nutrient Mixture (DMEM)/ F12 Ham, supplemented with 1% L-Glutamine-Penicillin-Streptomycin, 1% amphtotericin B solution and 10% FBS. On the fifth day after plating of BeWo cells onto the transwell, cells were transduced with shRNA lentiviral particles (or not transduced as a control). PLKO1 non-targeting shRNA (Sigma), or IL6 shRNAs TRCN0000059205 or TRCN0000059206 (Sigma), were added above and below the barrier BEWO media. After two days, media was removed and nanoparticles were added: pre-prepared nanoparticles were thawed and sonicated (bath sonicator) for 30 minutes. Media under the barrier was replaced with neuroprogenitor media comprising: 72% DMEM high glucose (Sigma), 24% DMEM/F12 + Glutamax (Thermo Fisher), 1% Glutamax (Thermo Fisher), 1% Penicillin/Streptomycin (Sigma) and 1% B27 (Thermo Fisher). 500μl of nanoparticles was added to the top of the barrier (or BEWO media without serum as a control). The following day, transepithelial/transendothelial electrical resistance (TEER) measurements were taken in the media on top of the barrier. Then, the media under the barrier was collected and snap-frozen in liquid nitrogen.

To study the effects on NPC differentiation from the conditioned media neurospheres were dissociated using accutase (Sigma) then placed in media without mitogens. 1 x 10^5 cells were then seeded onto 13mm PDL/laminin coated glass coverslips and allowed to adhere for 24 hours after which their media was replaced with NPC differentiation media conditioned in the BeWo barrier model plus/minus IL-6 shRNAs then cultured until day 7 of differentiation.

IL-6 antibody blocking experiment.

In another set of experiments BeWo barrier conditioned media was added to the cells, together with an anti-IL-6 antibody or relevant IgG control, at a concentration of 0.15 ug/ml (R&D systems). The blocking antibody remained in the culture for 6 days prior to removal of the media for measurement of IL-6 or fixation with 4% PFA for immunohistochemistry.

BeWo barrier immunoblot

Cells were lysed in RIPA buffer plus protease inhibitor (Roche). Protein was quantified using a BCA assay (Thermo Scientific) and resolved on polyacrylamide SDS-Tris-Glycine gels. Proteins were transferred onto PVDF membrane (Roche) and blocked using 10% non-fat milk in 0.1% TBS-T (Sigma). Incubation with primary antibody (mouse anti-HSP70 (Stressgen ♯C92F3A) 1:1000, mouse anti-p62 (Abnova ♯ H00008878-M01) 1:1000, mouse anti-p53 (Cell Signalling ♯2524) 1:1000, rabbit anti-LC3 (MBL ♯PM036) 1:1000, mouse anti-α-Tubulin (Sigma ♯T5168) 1:10,000) was carried out overnight at 4 °C in blocking buffer. Membranes were incubated with the appropriate HRP-labelled secondary antibody for 2 h at room temperature. Protein bands were visualized using Pierce Plus Substrate (Thermo).

Immunocytochemistry in NPCs

Cells were fixed in 4% paraformaldehyde (Fisher), with the exception of BeWo barrier staining where cells were fixed with ice cold 100% methanol. Cells were blocked at room temperature in PBS/10% goat serum/Triton X-100 0.1%. Primary antibodies were incubated overnight at 4 °C in PBS/2% goat serum/Triton X-100 0.1% using mouse anti-TUJ1 (Covance ♯MMS-435P) 1:1000, rabbit anti-GFAP (Dako ♯Z0334, Lot 20015408) 1:1000, chicken anti-GFAP (Abcam ♯Ab4674, Lot 2670366) 1:2000, rabbit anti-phosphorylated H2A.X (Ser139) (Cell Signalling Technology, ♯9718) rabbit anti-EAAT1 (Novus Biologicals NBP1-20135) 1:200, mouse anti-SQSTM1 (Abnova

♯H00008878-M01) 1:500 and rabbit anti-LC3-II (Viva ♯VB2930) 1:300. Alexa Fluor (Life Tech) secondary antibodies were incubated at room temperature for 2 hours in PBS/1% goat serum/Triton X-100. Cells were co-stained with DAPI (Sigma) and mounted in Vectorshield (Vectorlabs). Images were taken using fluorescence Leica DM RB upright microscope and processed using Adobe Photoshop and Image J software.

GSH-Glo Glutathione Assay in NPCs

The GSH-Glo luminescent assay (Promega) was used to detect the amount of GSH in exposed NPC cells and was measured on a Promax glomax multi detection system.

Live Dead Cell Count in NPCs

The Live/Dead viability/cytotoxicity kit (Life Technologies) was used to determine the number of live cells in the NPC cultures post media transfer experiments. The number of live and dead NPC cells on coverslips was counted using a Leica DMRB (Leitz) fluorescence microscope and image J.

MTS Cell Proliferation Assay in NPCs

The CellTiter 96 Aqueous Non-Radioactive Cell Proliferation Assay (Promega) was used to determine the mitochondrial activity in NPC cells and was measured on a Promega glomax multi detection system.

Assessment of *GFAP* gene expression in differentiated NPCs

Total RNA was extracted from cells (RNeasy mini system, Qiagen) and treated with RNase-free DNase I (Roche). cDNA was generated using Multiscribe reverse transcriptase (Thermo) and then a pre-amplification step was carried out using Taqman PreAmp mastermix and gene specific primers (Thermo). qPCR was carried out using the Taqman Universal Master Mix and Taqman assays (Thermo). Applied Biosystems software was used for analysis and relative gene fold variations were compared to the values for *GAPDH* that acted as a housekeeping gene.

Assessment of gene expression in embryoid bodies by qPCR

Embryoid Bodies (EBs) were created from Shef3 hES cells and allowed to expand in culture for 4 days. Following this the EB media was removed and replaced with EB media conditioned under the BeWo barrier model. The EBs were removed from this on day 7 then total RNA was extracted. (RNeasy mini system, Qiagen), treated DNase I (Roche). cDNA was generated using Multiscribe reverse transcriptase (Thermo) and the qPCR was carried out using the Taqman Universal Master Mix and Taqman assays. Each 20µl a reaction contained 50 ng cDNA. Applied Biosystems software was used for analysis and relative gene fold variations were compared to the values for *GAPDH* that acted as a housekeeping gene.

Supplementary Table 2: Taqman gene expression assays

Gene	Taqman Assay ID
EOMES	Hs00172872_m1
GAPDH	Hs00266705_g1/Hs02758991_g1
GATA4	Hs00171403_m1
GFAP	Hs00909233_m1
HAND1	Hs02330376_s1
NESTIN	Hs00707120_s1
OCT 4	Hs03005111_g1
P53	Hs01034249_m1

Assessment of Embryoid Bodies by flow cytometry

Flow cytometry was used to assess the formation of the three germ layers from

embryoid bodies (EBs). EBs were harvested following media transfer exposure

on day 7 of expansion and dissociated using Accutase. Dissociated cells were then washed with

DPBS then fixed in 4% PFA. 10% NGS diluted in 0.1% PBS-Triton X100 was used for blocking.

Control samples were run for all primary and secondary antibodies prior to flow cytometry

assessment to check for cross reactivity and to determine levels of autofluorescence. Primary

antibodies used were 1:4000 Goat anti chicken SOX1 (Millipore AB5934) and 1:20 Goat anti

mouse Nestin (Abcam AB6320). Secondary antibodies used were 1:2000 Cy5 anti chicken (Abcam

AB97147) and 1:500 Alexa fluor 488 anti mouse IgG (Life Tech A11001). Flow cytometry

assessment was performed on a BD LSR Fortessa X20 using FlowJo software. The authors wish

to acknowledge the assistance of Dr. Andrew Herman and Sally Chappell and the University of

Bristol Faculty of Biomedical Sciences Flow Cytometry Facility.

ELISA

Analysis of IL-6, TNFα, RANTES and GM-CSF concentrations

Supernatant concentrations of IL-6, TNFa, RANTES and GM-CSF (all from R&D Systems),

obtained from BeWo barriers +/- nanoparticles or from astrocyte cultures +/- media conditioned by

the BeWo barrier were measured using ELISA. Cytokine / chemokine concentrations in the test

samples were evaluated with reference to the standard curves prepared using recombinant

cytokines of a known concentration.

Additional mouse in vivo methods

Immunofluorescence staining and analysis

Frozen sections were incubated in blocking solution containing 10% goat serum (Invitrogen) in

0.3% PBS-Triton X-100 (Sigma-Aldrich) at room temperature for 2 hours. Sections were stained

with primary antibody, Polyclonal Chicken Anti-GFAP (1:500 Abcam ♯Ab4674) or rabbit anti-

phosphorylated H2A.X (Ser139) (Cell Signalling Technology, ♯9718) (1:500) diluted in 2% goat serum in PBS-Triton X-100 and incubated at 4°C overnight. The sections were rinsed and washed (3x for 10min) in PBS and Triton X-100. Secondary antibody using Life Technology Alexa Fluor 488 Goat anti-chicken 1:500 dilution or Alexa Fluor 555 Goat anti-rabbit 1:500 dilution was incubated for 2 hours at room temperature. Following wash steps, sections were mounted with Vectashield mounting medium containing DAPI (Vector Laboratories) and coverslips applied.

GFAP immunofluorescence intensity was analysed using Image J software (NIH, Betheseda, US) in sagittal sections (20mm) in the hippocampal region of P0 mouse brains. Sections were imaged with a Zeiss Fluorescent microscope (Axio Imager Z1) using 20x/0.5Ph2 objective lens, connected to an Axiocam HRm camera powered by AxioVision software. Captured digital images were analysed using Image J software as described by (Karve et al., 2016; McCloy et al., 2014) whereby regions of interest (ROIs) containing GFAP positive fluorescing cells were traced, which measured selected areas and integrated densities. The corrected total cell fluorescence (CTCF) intensities were determined by subtracting the area of selected GFAP positive cells multiplied by the mean fluorescence of background readings from the integrated density of cells. CTCF = Integrated Density–(Area of selected cell x Mean fluorescence of background readings). Average CTCF values were calculated for 10 x GFAP positive cells and 5 x background levels in the hippocampal region of P0 mouse brains sections from each treatment group (3 sections per slide and 3 slides per animal). For quantification of γ-H2AX immunostained sections were viewed under a 63x objective lens on a Zeiss Aim-system confocal microscope. Within the area of the hippocampus each cell containing 4 or more foci was considered damaged and hence counted.

qPCR quantitation of STEAP4, GFAP and PTX3 mRNA expression in P0 whole mouse brain and hippocampus.

RNA was isolated using the NucleoSpin RNA II kit (Machery Nagel, UK) as per the manufacturer's instructions. Extracted RNA yield was quantified using a NanoDrop'ND-1000 UV-Vis spectrophotometer (Thermo Fisher Scientific, UK) and cDNA was synthesised using a High

Capacity cDNA archive kit (Applied Biosystems, UK). Analysis of gene expression was conducted using real time PCR with specific primer and probe sets (Applied Biosystems).

In order to quantify the expression of specific target genes of interest, samples were assayed in duplicate with either primers and probes for GAPDH and PTX3 with FastStart Universal Probe Master mix (Roche) or primers (STEAP4 and GFAP) with FastStart Universal Sybr Green Master mix (Roche). Quantitative real-time PCR reactions were performed in a StepOne Plus™ Real-Time PCR system (Applied Biosystems, UK) using the following cycling protocol: 95°C for 10min; 95°C for 10s and 60°C for 30s for 40 cycles.

Gene expression analysis was conducted by the relative quantitation method with cDNA synthesized from an LPS injected mouse brain, which was utilized as the standard that would induce expression of all target genes of interest. Following subsequent dilutions, a linear standard curve was created whereby cycle threshold (Ct) was relative to concentrations of transcripts to determine relative mRNA expression, as previously described by (Hennessy et al., 2015; Cunningham et al., 2005). GAPDH was used as the endogenous control gene and target genes of interest were standardised to GAPDH.

Supplementary Table 3: The sequences for the primers and probes for the qPCR in vivo mouse experiments.

Gene	Forward Primer	Reverse Primer
GFAP	CTCCAACCTCCAGATCCGAG	TCCACAGTCTTTACCAGATGT
STEAP4	TGCAAGCCGGCAGGTGTTTGT	TCCAGTGGGGTGAGCCCAAGA
PTX3	ACAACGAAATAGACAATGGACTTCAT	CTGGCGGCAGTCGCA; Probe, CCACCGAGGACCCCACGCC

References

Basak, R. & Bandyopadhyay, R. 2013. Encapsulation of hydrophobic drugs in Pluronic F127 micelles: effects of drug hydrophobicity, solution temperature, and pH. *Langmuir,* 29(13), pp 4350-6.

Bhabra, G., Sood, A., Fisher, B., Cartwright, L., Saunders, M., Evans, W. H., . . . Case, C. P. 2009. Nanoparticles can cause DNA damage across a cellular barrier. *Nat Nanotechnol,* 4(12), pp 876-83.

Bode, C. J., Jin, H., Rytting, E., Silverstein, P. S., Young, A. M. & Audus, K. L. 2006. In vitro models for studying trophoblast transcellular transport. *Methods Mol Med,* 122(225-39.

Cunningham, C., Wilcockson, D. C., Campion, S., Lunnon, K. & Perry, V. H. 2005. Central and systemic endotoxin challenges exacerbate the local inflammatory response and increase neuronal death during chronic neurodegeneration. *J Neurosci,* 25(40), pp 9275-84.

Hennessy, E., Griffin, E. W. & Cunningham, C. 2015. Astrocytes Are Primed by Chronic Neurodegeneration to Produce Exaggerated Chemokine and Cell Infiltration Responses to Acute Stimulation with the Cytokines IL-1beta and TNF-alpha. *J Neurosci,* 35(22), pp 8411-22.

Karve, I. P., Zhang, M., Habgood, M., Frugier, T., Brody, K. M., Sashindranath, M., . . . Crack, P. J. 2016. Ablation of Type-1 IFN Signaling in Hematopoietic Cells Confers Protection Following Traumatic Brain Injury. *eNeuro,* 3(1), pp.

Liu, J., He, Y., Zhang, J., Li, J., Yu, X., Cao, Z., . . . Hong, Z. 2016. Functionalized nanocarrier combined seizure-specific vector with P-glycoprotein modulation property for antiepileptic drug delivery. *Biomaterials,* 74(64-76.

McCloy, R. A., Rogers, S., Caldon, C. E., Lorca, T., Castro, A. & Burgess, A. 2014. Partial inhibition of Cdk1 in G 2 phase overrides the SAC and decouples mitotic events. *Cell Cycle,* 13(9), pp 1400-12.

Parry, M. C., Bhabra, G., Sood, A., Machado, F., Cartwright, L., Saunders, M., . . . Case, C. P. 2010. Thresholds for indirect DNA damage across cellular barriers for orthopaedic biomaterials. *Biomaterials,* 31(16), pp 4477-83.

Raghunathan, V. K., Devey, M., Hawkins, S., Hails, L., Davis, S. A., Mann, S., . . . Case, C. P. 2013. Influence of particle size and reactive oxygen species on cobalt chrome nanoparticle-mediated genotoxicity. *Biomaterials,* 34(14), pp 3559-70.

Sood, A., Salih, S., Roh, D., Lacharme-Lora, L., Parry, M., Hardiman, B., . . . Case, C. P. 2011. Signalling of DNA damage and cytokines across cell barriers exposed to nanoparticles depends on barrier thickness. *Nat Nanotechnol,* 6(12), pp 824-33.